Temperature Effects on Sulfuric Acid Aerosol Nucleation and Growth: Initial Results from the TANGENT Study

Lee Tiszenkel[1], Chris Stangl[2], Justin Krasnomowitz[2], Qi Ouyang[1], Huan Yu[3], Michael J. Apsokardu[2], Murray V. Johnston[2], Shan-Hu Lee[1,4,*]

[1]Department of Atmospheric Science, University of Alabama in Huntsville, Huntsville, AL
[2]Department of Chemistry and Biochemistry, University of Delaware, Newark, DE
[3]School of Environmental Science and Engineering, Nanjing University of Information Science and Technology, Nanjing, China
[4]Department of Environmental Science and Engineering, Fudan University, Shanghai, China

Correspondence to: Shan-Hu Lee (shanhu.lee@uah.edu)

Abstract. New particle formation (NPF) consists of two steps: nucleation and subsequent growth. At present, chemical and physical mechanisms that govern these two processes are not well understood. Here, we report initial results obtained from the TANGENT (Tandem Aerosol Nucleation and Growth Environment Tube) experiments. The TANGENT apparatus enables us to study these two processes independently. The present study focuses on the effects of temperature on sulfuric acid nucleation and further growth. Our results show that lower temperatures enhance both the nucleation and growth rate. However, under temperatures below 268 K the effects of temperature on the nucleation rate become less significant and the nucleation rate becomes less dependent on RH, indicating that particle formation in the conditions of our flow tube takes place via barrierless nucleation at lower temperatures. We also examined the growth of newly formed particles under differing temperature conditions for nucleation and further growth. Our results show that newly nucleated clusters formed at low temperatures can indeed survive evaporation and grow in a warmer environment in the presence of SO_2 and ozone, and potentially other contaminant vapors. These results also imply that some heterogeneous reactions involving nanoparticles affect nucleation and growth of newly formed particles.

1. Introduction

Atmospheric nanoparticles affect human health and air quality. Newly formed particles can contribute to approximately 30-70% of cloud condensation nuclei (CCN) in the atmosphere (Merikanto et al., 2009;Wang and Penner, 2009;Yu and Luo, 2009;Gordon et al., 2017). NPF takes place via two steps: initial nucleation (formation of critical clusters) and subsequent growth of nucleated clusters (Kulmala et al., 2013). At present, chemical and physical mechanisms that govern these two processes, as well as the identity of chemical precursors involved in these processes, are still not well understood (Zhang et al., 2012;Yu et al., 2017b). Current global models fail to represent NPF in the atmosphere for a wide range of temperature and RH conditions and for different emissions of biogenic and anthropogenic precursors due to a lack of observations. For example, models predict frequent NPF during the summer in mixed deciduous forests in the United States (Yu et al., 2015), while field

observations show an absence of NPF in this region (Kanawade et al., 2011;Lee et al., 2016). Also, current NPF theories are unable to explain the frequent NPF observed in extremely polluted megacities (Yu et al., 2017b;Kulmala et al., 2017).

Temperature and RH are the key thermodynamic properties of aerosol formation and growth (Seinfeld and Pandis, 2016). Nucleation rate (J) is a function of temperature and the Gibbs free energy barrier of cluster formation. At lower temperatures, Gibbs free energy barriers become lower and critical cluster diameters become smaller. Condensational species can affect aerosol growth differently at different temperatures because their saturation vapor pressures are dependent on temperature. For water, RH is the same as saturation ratio and chemical activity. Laboratory experiments of aerosol nucleation and growth as a function of temperature and RH remain limited, although these observations are critically needed in global models to correctly parameterize NPF under various altitude, latitude and seasonal conditions. Aerosol nucleation experiments are extremely challenging due to various experimental difficulties, including contamination of base compounds (Erupe et al., 2011;Yu et al., 2012). At present there is a lack of consistency between different experiments from different groups and even from the same groups using the same experimental setup. The lack of reproducibility and consistency of the nucleation experiments greatly hinders our understanding of nucleation mechanisms.

(Duplissy et al., 2016) conducted studies of binary homogeneous nucleation of sulfuric acid and water, with and without ions in the CLOUD (Cosmics Leaving OUtdoor Droplets) chamber at different temperatures ranging from 207 to 299 K and RH between 11% - 58%. At lower temperatures both ion nucleation and neutral binary nucleation are at the kinetic regime, while at higher temperatures J is strongly dependent on [H_2SO_4], indicating there are high Gibbs free-energy barriers at these temperatures. At the nucleation regime, nucleation rates are strongly dependent on RH. Kürten et al. (2016) reported the temperature dependence of ternary nucleation in the CLOUD chamber, at the temperature from 208 to 298 K, [H_2SO_4] between 10^5 and 10^9 cm^{-3}, and [NH_3] up to ~1400 pptv. At 208 K, J reached the threshold of 1 cm^{-3} s^{-1} at a [H_2SO_4] of ~3×10^6 cm^{-3} for the binary case, and at [H_2SO_4] of ~5×10^5 cm^{-3} for the ternary case with [NH_3] of 5 pptv. At 298 K, RH has strong effects on the measured J for both charged and neutral ternary nucleation, because this increase in RH could lead to a displacement of NH_3 from the stainless-steel walls in the CLOUD chamber and lead to an elevated NH_3 background level and consequently to higher J.

Laboratory experiments of growth rates (GR) of newly nucleated particles are very sparse. (Skrabalova et al., 2014) studied GR of newly formed particles in a flow tube at the temperature between 283 to 303 K and RH of 1% and 30%, designated as "dry" and "wet" conditions, respectively. [H_2SO_4] was varied between 2×10^8 cm^{-3} and 1.4×10^{10} cm^{-3}. They found different effects of RH on GR; at [H_2SO_4] below 10^9 cm^{-3}, growth is promoted in drier conditions, whereas at [H_2SO_4] higher than 10^9 cm^{-3}, growth favours wetter conditions. Yu et al. (2017a) performed flow tube experiments of sulfuric acid aerosol nucleation, at the temperature from 248 to 313 K and RH from 1% to 79%, under minimal base concentrations ([NH_3] < 23 pptv, methylamine < 1.5 pptv, and dimethylamine < 0.52 pptv). Their study provides for the first time the temperature and RH dependence of both J and GR. J shows the following dependence within the experimental conditions:

$$J = 10^{41.8}[RA]^3[RH]e^{\frac{-2.4\times10^4}{T}}, \qquad (1)$$

where RA is relative acidity (or saturation ratio) of sulfuric acid, and T temperature. Their results show that *GR* is independent of temperature below 290 K, but significantly decreases at temperatures above 290 K. RH has a moderate effect on *GR*.

At present, there is still no clear evidence from atmospheric observations that demonstrates "causal effects" of temperature and RH on NPF. Recent CLOUD studies have shown that oxygenated organics formed from BVOCs can grow newly nucleated particles in a wide range of tropospheric temperatures (Stolzenburg et al., 2018). This is because gas phase autooxidation reactions involved in the formation of HOMs usually have strong temperature dependencies, with higher reaction rates at higher temperatures (Frege et al., 2018), whereas nucleation is favoured at lower temperatures.

Another important perspective of temperature effects on NPF is the effects of temperature on evaporation of newly nucleated clusters and nanoparticles that have undergone transport to differing temperature conditions for further growth. Boundary layer particle concentrations in the marine regions have been shown to be a result of sulfuric acid-driven nucleation of nanoparticles in the free troposphere as a result of oxidation of upwardly transported and oceanic dimethylsulfide. These particles then undergo downward transport to become reservoirs of nanoparticles in the boundary layer. This has been observed and modelled by several groups over the previous decades (Russell et al., 1994;Raes, 1995;Clarke, 1993).

The lack of local NPF events in Amazon forests has been a confounding observation for many years (Rizzo et al., 2018) and yet there are reservoirs of nuclei mode particles at the surface which do not form typical "banana" plots of aerosol size distributions observed elsewhere (Martin et al., 2016). Understanding the origin of these nuclei mode particles has been a subject of recent studies. (Wang et al., 2016) reported that while NPF does not take place in Amazon forests at the surface level during the dry and wet season, NPF takes place in the colder free troposphere; these newly formed particles can be transported down to the boundary layer to become a reservoir of nanoparticles at the surface. This downward transport process is very similar to the above-mentioned marine boundary layer nanoparticle processes (Russell et al., 1994; Raes et al., 1995; Clarke et al., 1993). A subsequent question is thus whether newly nucleated clusters and nanoparticles in the free troposphere can survive evaporation during their transport to the warmer boundary region.

At present, the temperature effects on the growth of newly formed particles crossing different temperature regions have not been examined in a controlled laboratory environment. In order to address this shortcoming in laboratory experiments of this relatively common phenomenon, we have constructed the TANGENT apparatus, consisting of a temperature- and RH-controlled nucleation flow tube that permits study of gas-to-particle conversion over a wide parameter space. This nucleation region is connected to a room temperature growth tube where conditions for further growth of these nanoparticles can differ dramatically from those of their nucleation. With the suite of instruments monitoring precursor gases as well as particle size distributions from sub-3 nm up to CCN sizes at key areas of the flow apparatus, the critical processes that atmospheric nanoparticles undergo can be studied and parameterized with TANGENT.

Here, we present the initial results of the TANGENT experiments conducted during the Intensive Observation Period (IOP) study in June and July 2018. In the present study, we report the temperature effects on *J* and *GR* of sub-2 nm particles in the nucleation tube. We also discuss how temperature differences in the nucleation and growth tube affect the potential evaporation of newly nucleated clusters while these clusters are transported from the colder to the warmer temperature region.

2. Methods

2.1 The TANGENT Experimental Setup

Figure 1 shows the schematic diagram of the TANGENT apparatus. The TANGENT consists of the two flow tubes (FT) to enable studies of nucleation (FT-1) and subsequent growth (FT-2). The nucleation tube was built by the University of Alabama

5 in Huntsville, and the growth tube by University of Delaware. TANGENT allows for nucleation to be observed as a separate process from growth; with a short residence time (45 s), precise temperature control, and the ability to produce H_2SO_4 at concentrations spanning 10^6 to 10^9 cm^{-3}, FT-1 is able to nucleate and monitor particles from precursor gases at a variety of conditions. After particles are nucleated in FT-1 where size distributions are recorded, particles are then transported to the growth tube (FT-2), where the particles undergo further growth at room temperature for a longer residence time (4 min) with

10 the ability to precisely control other trace gases in the growth environment. According to our knowledge, this is the first flow tube experimental setup that allows for aerosol nucleation and growth processes to be investigated independently but at the same time.

The experimental setup of the nucleation region (FT-1) was based on (Benson et al., 2009;Benson et al., 2008;Erupe et al., 2011;Young et al., 2008b;Yu et al., 2012;Yu et al., 2017a;Benson et al., 2011). It consists a photolysis region where H_2SO_4 is

15 generated photochemically and monitored followed by a temperature-controlled nucleation tube. In the photolysis region, OH radicals were produced via photodissociation of water vapor in a quartz tube using a mercury lamp (Pen-Ray Model 11SC-1). The mercury lamp was located in a temperature-controlled enclosure filled with a constant nitrogen flow. UV intensity was adjusted with an aperture over the slit in the enclosure exposing the quartz tube to the UV lamp. UV intensity was monitored with a CsI phototube (Hamamatsu Model R5764) and picoammeter (Keithley 6732). Measurements of UV intensity were taken

20 to ensure consistency between experimental trials. SO_2, O_2 and N_2 gases were introduced to the flow tube immediately after the photolysis region. H_2SO_4 forms from the $SO_2 + OH$ reaction. Heating tape was applied to the H_2SO_4 production region to suppress nucleation prior to entering the temperature-controlled nucleation zone. The H_2SO_4 production region was monitored with a condensation particle counter (CPC, TSI 3776) and particle sizing magnifier (PSM, Airmodus A09) to ensure no particles were formed before the flow entered the nucleation region.

25 H_2SO_4 concentrations at the beginning of the nucleation tube were measured with a nitrate-based chemical ionization mass spectrometer (CIMS) based on (Eisele and Tanner, 1993) continuously during the experiments. Calibration of $[H_2SO_4]$ with the nitrate-CIMS was described previously by (Young et al., 2008a). The CIMS was operated with an inlet flow of 5.0 SLPM and an ion-molecule reaction time of 0.05 s. The lower limit of detection was calculated to be $\sim 1 \times 10^5$ cm^{-3}.

No base compounds were added, but base compounds were present in the flow tube as impurities likely generated from

30 deionized water used for H_2SO_4 production and RH control (Erupe et al., 2011;Yu et al., 2012). NH_3 and amines were not measured during the 2018 IOP, but they were measured under very similar experimental conditions during the entire 2017 IOP with an ethanol-CIMS at the beginning of the nucleation tube (You et al., 2014;Yu and Lee, 2012). Detection limits of

NH$_3$/amines in our CIMS were pptv or sub-pptv with a 1-min integration, as previously discussed elsewhere (Benson et al., 2010;Erupe et al., 2011;You et al., 2014;Yu and Lee, 2012).

The nucleation tube is an 80 cm long Pyrex glass tube with an i.d. of 4.85 cm. The temperature of the nucleation tube was controlled with a circulating bath and a water-based potassium formate heat transfer fluid (Dynalene HC-50, Dynalene, Inc.) to adjust the temperature between 258 and 297 K. RH was adjusted by directing some of the dry nitrogen makeup flow through deionized water in a water bubbler. Thus, in our experimental setup, changes in RH in the nucleation tube did not affect the OH radical concentrations in the photolysis region. Temperature and RH probes (CS-215, Campbell Scientific) were used to monitor the conditions at the beginning of the photolysis region, as well as at the end of the nucleation region. An additional temperature and RH probe (Traceable, Fisher Scientific) was applied inside the nucleation tube to confirm the RH. Residence time in the nucleation region (FT-1) was 45 s.

Particle concentrations at the exit of FT-1 were measured with a PSM (Vanhanen et al., 2011). The PSM saturator flow was operated with a 240-step cycle between 0.1 - 0.9 SLPM at a rate of 1 s per step, giving saturator flow dependent cut-off sizes between 1.26 nm and 2.85 nm. These cut-offs were resolved to six size bins in an inversion method based on (Lehtipalo et al., 2014) producing size distributions with six size bins: 1.26 - 1.53 nm, 1.53 - 1.79 nm, 1.79 - 2.06 nm, 2.06 - 2.32 nm, 2.32 - 2.59 nm, and 2.59 - 2.85 nm. Particle concentrations were also monitored with a scanning mobility particle sizer (SMPS) consisting of a differential mobility analyser (DMA, TSI 3080) and a CPC (TSI 3776). However, under the typical experimental conditions, particles above 3 nm in diameter did not appear even with the most favourable conditions for nucleation and growth (e.g., high [H$_2$SO$_4$], high RH and low temperature).

During the experiments, [H$_2$SO$_4$] was varied by adjusting the aperture on the mercury lamp housing (hence varying [OH]) at a fixed [SO$_2$], allowing for a range of [H$_2$SO$_4$] spanning roughly one order of magnitude for a given dilution of SO$_2$. [H$_2$SO$_4$] was further varied by adjusting the SO$_2$ dilution, allowing for measurements spanning [H$_2$SO$_4$] of 10^6 to 10^9 cm^{-3}. The PSM measurements showed that each experimental condition was "stabilized" typically after ~30 min for a specific set of [H$_2$SO$_4$], RH and temperature.

The photolysis and nucleation tubes were cleaned thoroughly with deionized water, citric acid solution and ethanol and allowed to dry for 24 hours while heated to 60 °C with pure N$_2$ flowing through the flow tube. Between experiments, the photolysis and nucleation tubes were continuously flushed with dry vaporized liquid nitrogen. A constant flow of N$_2$ was passed through the experimental apparatus at all times during the IOP to ensure that the conditions inside the tube would remain constant and there would be no intrusion of room air.

The nucleated clusters (smaller than 2 nm) were transported to the growth tube (FT-2) for further growth with an extended residence time (4 min). FT-1 and FT-2 were coupled with an 8-inch stainless steel tube with additional inlet ports for injection of ozone, zero air and SO$_2$. The growth tube was described by (Krasnomowitz et al., 2019;Stangl et al., 2019). The growth tube consists of a 1.52 m long and 0.2 m inner diameter fused quartz tube fitted with stainless steel funnels on each end that reduce the inner diameter down to 0.051 m. The total volume of the tube and entrance and exit funnels is 52.4 L, giving a surface-to-volume ratio of 0.24 cm^{-1}. The 8-inch straight tube fitting allows carrier/reactant gases to enter the tube via an axial

inlet port and continuous flow through the entire length of the reactor during the course of an experiment. The end of the tube was attached to an ozone monitor (Thermo Scientific 49i), a hygrometer (Traceable, Fisher Scientific), and an SMPS (TSI 3938, 3788).

FT-2 has several ports at the inlet to inject additional gases in to the system to observe their effects on further growth of freshly

5   nucleated particles. Ozone was added to FT-2 using the calibration ozone generator on a Thermo Scientific 49i. Ozone was varied in FT-2 by adjusting the UV intensity of the calibration lamp. The residence time in FT-2 could be changed by varying the flow of zero air in to FT-2. During a typical experimental run using both FT-1 and FT-2, conditions would only be changed in FT-2, with temperature, RH and precursor species in FT-1 held constant throughout the entire experiment. The experiments undertaken in this study measured two effects in the system: the effect of changing temperature in the nucleation region as

10   well as the effect of varying ozone (in the co-presence of SO_2) in the growth region.

2.2 Calculations of Nucleation (J) and Growth Rate (GR)

Calculations of J were made based on (Yu et al., 2017a). Briefly, J was calculated according to the following approximation:

$$J_0 \approx N_{tot} \times nk_L, \tag{2}$$

where J_0 represents the nucleation rate corresponding to the initial sulfuric acid concentration ($[H_2SO_4]_0$) measured at the

15   beginning of the nucleation tube, N_{tot} the total number concentration of particles detected at the end of the nucleation region, n the nucleation theorem power and k_L the diffusion-limited, pseudo first-order wall loss coefficient (Hanson and Eisele, 2000). The nucleation theorem power n was experimentally determined for each set of experiments by the linear fit of Log N_{tot} vs. Log $[H_2SO_4]_0$, Our k_L was typically 0.01 s^{-1}. Eq. 2 allows us to obtain J_0 at different $[H_2SO_4]_0$ using n and N_{tot} of the formed clusters (all smaller than 2 nm in the present study).

20   To calculate GR, the critical cluster size was determined experimentally, with the critical cluster size corresponding to the y-intercept of the linear fit between the mean particle diameter, D_p, and the $[H_2SO_4]_0$ (e.g., Fig. 3). D_p was obtained using the inversion of the PSM size distribution measured at the end of FT-1. GR was calculated by the difference between the critical size and D_p divided by the nucleation time.

The growth rate factor k_G is defined as the growth rate enhancement over 1 pptv H_2SO_4 causing 1 nm hr^{-1} of growth. The

25   collision limited condensation of H_2SO_4 of 1 pptv contributes roughly 1 nm hr^{-1} of growth rate at a temperature of 298 K (Nieminen et al., 2011). Thus, the k_G is an indicator of the deviation of the actual growth rate compared to this conventional collision-limited GR. The k_G were determined by the expression derived by (Yu et al., 2017a):

$$k_G = \frac{\Delta D_{p,tr} \times 10^7 cm^{-3}}{[H_2SO_4]_0} \frac{k_L}{1-e^{-nk_L t_r}}, \tag{3}$$

Where $\Delta D_{p,tr}$ represents the change in diameter over the residence time (t_r) in the nucleation tube (FT-1). $\frac{\Delta D_{p,tr}}{[H_2SO_4]_0}$ was

30   experimentally determined from the slope of the D_p vs. $[H_2SO_4]_0$ plot (e.g., Fig. 3). $\frac{k_L \times 10^7 cm^{-3}}{1-e^{-nk_L t_r}}$ can be calculated from n and k_l values. The k_G is the product of this slope and $\frac{k_L \times 10^7 cm^{-3}}{1-e^{-nk_L t_r}}$. Extrapolation to the y-axis of Figure 3 gives a value for the

critical cluster diameter. $\Delta D_{p,tr} = 0$ for the critical cluster and thus $D_{p, critical}$ will be equal to the y-intercept of the linear fit of each data set.

2.3 Uncertainty analysis

The uncertainties in the J_0 calculation arise from uncertainties in CIMS H_2SO_4 measurements, measurements of particle concentrations in the PSM and the size inversion from PSM-measured number concentrations. The uncertainty in the H_2SO_4 CIMS is approximately 60% (Erupe et al., 2010;Eisele and Tanner, 1993;Benson et al., 2008;Benson et al., 2009;Kürten et al., 2012;Petäjä et al., 2009). The wall loss calculation has ±7% uncertainty (Hanson and Eisele, 2000). The measurement error in the PSM size distribution, based on the standard error calculated between run-to-run experiments under identical conditions, is ±26%. The uncertainties in inversion of the particle diameter from the PSM measurement are estimated around 12% (or ±0.2 nm) for inorganic particles in the size range observed in this experiment (Lehtipalo et al., 2014;Lehtipalo et al., 2016;Kulmala et al., 2013;Yu et al., 2017a). Propagation of the errors in sulfuric acid measurement, wall loss, and the PSM measurements results in an overall uncertainty of ±65.5% in the calculation of J_0.

3. Results and discussion

3.1. Nucleation and growth in FT-1

Table 1 shows the typical experimental conditions used in the FT-1 (nucleation tube) and FT-2 (growth tube) during the 2018 IOP study. In the nucleation tube, temperature was varied from 258 to 297 K and RH from 4% to 85%. $[H_2SO_4]$ spanned from 10^6 to 10^8 cm^{-3}, corresponding to RA of 10^{-5} to 10^{-2}. RA was calculated using the sulfuric acid saturation vapor pressures provided by (Vehkamaki et al., 2002). NH_3 and amine measurements not taken during this study, but they were undertaken during the 2017 IOP campaign using the same experimental apparatus, precursor gases and cleaning schedule as the 2018 campaign that is the concern of this study. The CIMS-measured NH_3 (during the 2017 IOP) was 14.2 ± 6.7 ppt (Fig. 2). Thus, the ratio of $[NH_3]/[H_2SO_4]$ ranged from 0.6 to 268. According to (Schobesberger et al., 2015) and (Dunne et al., 2016), these ratios represent ternary nucleation and some nucleation in a transition regime between binary and ternary, when considering only the effects of NH_3 (without amines). Amine concentrations were detected at levels ranging from 4.5 ± 2.60 ppt for C1 amines to 44.8 ± 41.8 for C2 amines (Fig. 2). Overall, the measured nucleation rates ranged from 10 - 10^5 cm^{-3} at higher temperatures and lower $[H_2SO_4]$ up to 10^5 cm^{-3} at lower temperatures and higher $[H_2SO_4]$. The observed GR ranged from 1 to 80 nm h^{-1}. The growth tube (FT-2) was kept at room temperature (297 K) and dry conditions (RH of 10%). SO_2 was added in the range from 100 ppbv to 5 ppmv and ozone from 0 to 248 ppbv.

Figure 3 shows the measured D_p with the PSM at the end of FT-1 as a function of the initial $[H_2SO_4]_0$ at the temperature between 258 and 297 K. $[H_2SO_4]_0$ was varied from 8×10^6 cm^{-3} to 7×10^7 cm^{-3}. The RH was kept in relatively narrow range between 20% and 30%. The y-intercept in Fig. 3 indicates the critical cluster diameter was estimated to be between 1.6-1.7

nm depending on temperature, with lower temperatures resulting in smaller critical cluster diameters. However, since the PSM inversion that determines D_p has an uncertainty of ±0.2 nm, it is difficult to discuss the temperature trends of the critical cluster diameter. This critical size is consistent with the studies of (Kulmala et al., 2013) and (Almeida et al., 2013), which determined critical cluster diameters of 1.5 ± 0.3 nm and 1.7 nm, respectively. For a given $[H_2SO_4]_0$, the mean D_p at the end of the 45

5   second residence time in FT-1 was larger for lower temperatures. Previously, (Glasoe et al., 2015;Yu et al., 2017a) have also shown increasing GR with increasing $[H_2SO_4]$ from flow tube experiments. The slope of D_p vs. $[H_2SO_4]_0$ increased with each 10 degree decrease in temperature over the course of these experiments. Thus, the growth rate factor k_G also increased with subsequent temperature decreases (e.g., from 1.27 at 297 K to 12.6 at 258 K). These results indicate that lower temperatures promote the faster growth of particles due to the reduction in saturation vapor pressures of H_2SO_4 at lower temperatures.

10   Figure 4 shows the relationship of Log J vs. Log RA for different temperatures. Experiments were conducted at 10 K intervals, starting from 297 K down to 258 K for RH between 41% and 45%. Across all temperature and RH experiments conducted, in general, J values were shifted 2 to 3 orders of magnitude above previous literature values of flow tube nucleation studies (Brus et al., 2010;Yu et al., 2017a) and 4 to 5 orders of magnitude above CLOUD measurements of H_2SO_4 nucleation as shown in the figure using CLOUD data from (Dunne et al., 2016). This upward shift was consistent across trials. Based on our measured

15   NH_3 and amine concentrations (Fig. 2), this upward shift is consistent with the nucleation rate enhancement due to synergistic effects of NH_3 concentrations on the order of 20 to 30 pptv and dimethylamine concentrations on the order of 5 ppt reported by other studies (Glasoe et al., 2015). There was a consistent relationship between Log J and Log RA. Except for 288 K and 297 K, where the slope of Log J vs. Log RA was approximately 2, slope was 3 for all trials, with the best-fit lines shifting towards higher values of RA as temperature decreased. Hanson and colleagues provided comprehensive analysis of Log J vs.

20   Log RA (or Log $[H_2SO_4]$) obtained from flow tube studies (Glasoe et al., 2015;Zollner et al., 2012). In general, flow tube studies from various groups have shown slopes between 3-6 for the ternary system (Glasoe et al., 2015;Zollner et al., 2012;Brus et al., 2010;Berndt et al., 2014;Erupe et al., 2011;Yu et al., 2012;Hanson et al., 2017). Using the CLOUD experiments, (Dunne et al., 2016;Almeida et al., 2013;Kirkby et al., 2011) also showed the slope of 3 for the ternary system. This slope is consistent with the base-stabilization mechanism provided by (Chen et al., 2012;Jen et al., 2014;Jen et al., 2016) that the bottleneck

25   clusters contain 3-4 H_2SO_4 molecules with at least one base molecule. It was previously believed that the slope of Log J vs. Log RA dictates the amount of H_2SO_4 molecules present in the critical cluster based on classical nucleation theory (CNT) (Kashchiev, 1982;McGraw and Zhang, 2008), which then would imply here that the critical cluster contains three H_2SO_4 molecules for the ternary system. However, more recent work by (Malila et al., 2013;Vehkamäki et al., 2012) has shown that this conclusion may be an oversimplification of the mechanism of particle formation resulting from an application of CNT

30   with an incomplete understanding of the free energy maxima and minima.

Figure 5 shows the measured J as a function of temperature for $[H_2SO_4]$ between 2×10^7 and 3×10^7 cm^{-3} and RH between 15% to 45%. J increased with the decreasing temperature in the temperature range above 268 K. The higher J at lower temperatures is consistent with predictions from CNT (Seinfeld and Pandis, 2016). However, a shift in slope is visible around 268 K, indicating that the dependence of J on temperature becomes less significant at low temperatures. The variation seen across RH

at higher temperatures also becomes negligible below this temperature. Thus, these results indicate that at temperatures below 268 K, Gibbs free energy barriers are reduced significantly.

3.2. TANGENT experiments: Further growth of clusters in FT-2:

In order to determine whether newly formed particles nucleated at lower temperatures can survive downward transport to warmer temperature conditions, we conducted two tests (Figs. 6 & 7): the first test had a much lower temperature in FT-1 (268 K) than in FT-2 (297 K) and the second test had the same temperature (297 K) in both tubes. Figure 8 shows the *GR* and particle survival percentage, calculated by dividing the particle concentration at the end of FT-2 by the particle concentration at the end of FT-1. During the first test (Fig. 6), the average particle concentration coming out of FT-1 was 2×10^5 cm^{-3} with a median diameter of 1.9 nm at [H_2SO_4]$_0$ of 6×10^7 cm^{-3} and RH of 10%. These newly formed particles were further mixed with an additional zero air flow at a 1:6 dilution. The [SO_2] was 83 ppbv and the ozone level was varied from 0 to 248 ppbv in FT-2. No particles were observed coming out of FT-2 when ozone was absent, indicating that SO_2 alone does not cause nucleation and growth of clusters. However, in the presence of ozone and SO_2, continuous nucleation and further growth of transported clusters took place in FT-2. The particle concentration measured at the end of FT-2 was closely correlated with the ozone concentration: the particle concentration ranged from 3×10^2 cm^{-3} (with D_p of 2.8 nm) at the lowest ozone of 28 ppbv up to 5×10^4 cm^{-3} (D_p of 3.4 nm) at the maximum ozone of 248 ppbv. Thus, the particle concentration in FT-2 at the highest ozone was even greater than that coming out of FT-1 after dilution, indicating that a high ozone load resulted in additional nucleation and the further growth of clusters in FT-2; this is indicated by the greater than 100% particle survival shown in Figure 8b. This could be the result of the remaining H_2SO_4 vapour passing through to FT-2, but we excluded this possibility. After considering wall loss in FT-1 and the 1:6 dilution FT-2, [H_2SO_4] in FT-2 was estimated to be 1.15×10^6 cm^{-3}, which can result in *J* only on the order of 10^1 cm^{-3} s^{-1} at room temperature and the dry condition, as shown from the results obtained in FT-1 (e.g., Fig. 4). However, the measured formation rate (*J*) of particles in FT-2 was 190 cm^{-3}s^{-1}, in contrast to this estimation. There was another possibility that ozone reacted with possible organic impurities in FT-2 to produce OH, which oxidized SO_2 to produce H_2SO_4 and nucleated in FT-2, but no organics were added in our experiments. It is not clear at present what is the cause of nucleation in FT-2 and this requires future study. However, it was clear that the co-presence of ozone and SO_2 was an important factor in preventing evaporation of newly formed particles and facilitated them to grow further at a higher temperature. The overall *GR* of particles in FT-2 was from 14.9 to 23.1 nm h^{-1}, depending on the ozone concentration. These results may imply some heterogeneous reactions occurring on acidic sulfuric acid clusters, in a similar way to form sulfate from oxidation reactions of SO_2 on acidic particles as proposed by (Hung and Hoffmann, 2015).

The second test was conducted with FT-1 and FT-2 both at a constant temperature of 297 K (Fig.7). FT-1 was held at a constant [H_2SO_4]$_0$ of 1.3×10^8 cm^{-3}. The total particle concentration out of FT-1 for this experiment was 1.7×10^5 cm^{-3} with a mean diameter of 1.9 nm. Aside from the higher [H_2SO_4]$_0$, which was necessary to produce the same particle concentration in the higher temperature FT-1, particle count and mean diameter were similar to the experiment with a cold FT-1. However, the size distributions in Figure 6a and Figure 7a indicate that there were more particles in the higher diameter size bins when the

temperature in FT-1 was lower. At the end of FT-2, particle concentration and size were again closely correlated with ozone concentration, ranging from 8.6×10^1 cm^{-3} ($D_p = 2.7$ nm) at the lowest ozone concentration up to 2.3×10^4 cm^{-3} ($D_p = 3.8$ nm) at the highest ozone load. These concentrations and sizes result in growth rates ranging from 12.0 to 28.1 nm hr^{-1}, indicating that the growth the highest ozone concentrations was faster during the constant temperature experiment. This was due to a greater

5 concentration of smaller particles formed at higher [H$_2$SO$_4$]$_0$ in the second test.

Examining the contrast between the temperature gradient (Fig. 6) and constant temperature (Fig. 7) experiments, as well as the comparison between the experiments' *GR* and particle survival in Figure 8, we see notable effects of temperature gradient on the survival of particles to the end of FT-2. While the average size at the end of the nucleation tube was similar in each experiment ($D_p = 1.9$ nm with 268 K FT-1, $D_p = 1.9$ nm with 298 K FT-1), we can see from the size distributions in each

10 experiment that the low-temperature FT-1 resulted in a greater concentration of particles in the larger size bins. These particles (once they are stabilized, e.g. by base compounds) are more thermodynamically stable and therefore have a greater ability to survive evaporation when transported to the warmer environment of FT-2. Particles formed in warmer environments have a greater energy barrier to overcome before they become stable enough to grow spontaneously (Lovejoy et al., 2004). Figure 8 shows that both the particle growth rate as well as the tendency for the particles to survive to the end of FT-2 was clearly

15 correlated with ozone concentration, indicating that the concentration of ozone in FT-2 was a critical factor in the persistence, growth and nucleation that occurred in FT-2 during these experiments.

The additional nucleation occurring in FT-2 in the co-presence of SO$_2$ and ozone cannot be explained by current knowledge. These results suggest some possible heterogeneous reactions involving SO$_2$ and ozone on acidic clusters. One possibility is the presence of alkaline species such as transition metal or high NH$_3$/amine concentrations that could increase the pH of the

20 particles, which can contribute to the production H$_2$SO$_4$ by SO$_2$ oxidation in the presence of ozone (Seinfeld and Pandis, 2016;Hung and Hoffmann, 2015). However, CLOUD studies have often found that particles nucleated in the presence of NH$_3$/amines remain acidic (Lawler et al., 2016). Understanding how SO$_2$ and ozone interact each other on the acidic nanoparticles to facilitate nucleation and growth will require future studies.

We also examined the additional effects of organics and base compounds on *GR* in FT-2. First, to see the effects of possible

25 impurities of organics, we used the growth rate parameterization from (Tröstl et al., 2016):

$$GR = kD_p[HOM]^p \tag{4}$$

Solving Eq. 4 for [HOM] using our observed growth rates of 12.0 to 28.1 nm hr^{-1}, $D_p = 1.9$ nm, $k = 5.2 \times 10^{-11}$ and $p = 1.424$ (Tröstl et al., 2016) results in a [HOM] of 2.8 to 3.8 pptv necessary to account for these growth rates. The amount of monoterpene required to produce that amount of HOMs was calculated using equation 16 from Trostl et al., 2016 solved for

30 [MT]:

$$[MT] = \frac{[HOM]*CS}{Y_1 k_1 [O_3]} \tag{5}$$

Using the yield of HOMs from ozonolysis of monoterpenes $Y_1 = 2.9\%$ (Kirkby et al., 2016), temperature dependent reaction rate of ozone and α-pinene $k_1 = 8.06 \times 10^{-17}$ (Khamaganov and Hites, 2001), and 10^{-3} for condensation sink (*CS*, calculated from

size distributions in FT-2) it would require between 100 and 1000 ppbv of monoterpenes to account for that concentration of HOMs. These high concentrations were very unlikely to be present in FT-2 considering the rigorous cleaning of the TANGENT apparatus as well as the lack of added monoterpenes to the system.

Second, to see the possible multicomponent growth due to the presence of ammonia in the system, we utilized the parameterization of multicomponent growth from equation (4) of (Lehtipalo et al., 2018):

$$GR = k_1[H_2SO_4]^a + k_2[H_2SO_4]^b[NH_3]^c + k_3[Org]^d \qquad (6)$$

Where k_1 and k_2 are 2.05×10^{-7} and 6.69×10^{-11}, respectively (Lehtipalo et al., 2018) and $a = b = c = d = 1$. Assuming [Org] = 0 for simplicity, and $[H_2SO_4]$ and $[NH_3]$ values from the temperature gradient experiment (1.15×10^6 cm^{-3} H_2SO_4, 14 ppt NH_3 estimated from 2017 IOP measurements), we should expect a GR of 0.24 nm hr^{-1}. However, this calculation only considers the presence of NH_3 in the system, when it is very likely that there were amines present at pptv levels (Fig. 2). (Glasoe et al., 2015) and (Yu et al., 2012) found synergistic effects on GR when both NH_3 and methylamine/dimethylamine are present that can enhance GR by 1 to 2 orders of magnitude, which would put these calculated GR values in range of the observed 23.1 nm hr^{-1} GR seen in the FT-2.

Also, cluster-cluster collision in the presence of stabilizing base compounds such as trace amines that were present in TANGENT can enhance growth by an order of magnitude (Lehtipalo et al., 2016). Thus, it seems that the observed high GRs in FT-2 were at least in some part due to multicomponent effects of base compounds and cluster-cluster collisional growth effects on GR, in addition to potential heterogeneous processes discussed above.

The chemical composition of the particles nucleated and grown in this experiment is an element that is likely to have an influence on their stability, growth, and survivability in a different environment. We did not measure chemical composition of clusters and particles in the present study. However, we can surmise the chemical composition of the particles in this study based on CLOUD studies that utilized APi-TOF instruments (Duplissy et al., 2016;Kirkby et al., 2011;Kürten et al., 2014). These studies, conducted in similar precursor conditions of H_2SO_4 and NH_3/amines at pptv levels, found that pure H_2SO_4 clusters did not exist beyond dimers and trimers at the lowest temperatures; NH_3 or amines particles consisting of H_2SO_4 molecules clustered with ammonia molecules at ratios up to 1:1 were common. It thus can be expected that the particles in this study had a similar chemical composition, and the presence of bases in these newly formed particles was a critical factor for their survival and further growth. This chemical composition is also consistent with above analysis about the GR in the FT-2, derived from the multicomponent nucleation and growth processes by (Lehtipalo et al., 2018).

4. Conclusions and Implications

We have conducted experiments to study the temperature dependence of aerosol nucleation and growth using the TANGENT setup. This setup consists of two flow tubes which enable us to study nucleation and subsequent growth independently. In the nucleation tube, temperature was varied from 258 to 297 K and RH from 4% to 85%. $[H_2SO_4]$ spanned 10^6 to 10^8 cm^{-3}, which corresponds to RA of 10^{-5} to 10^{-2}. Based on the measured $[NH_3]$ to $[H_2SO_4]$ ratios, it was most likely that nucleation took place

via the ternary process. The growth tube was kept at room temperature and the dry condition (RH of 10%). SO_2 was present at 100 ppbv to 5 ppmv and ozone at 0 to 248 ppbv.

Our results indicate that lower temperatures enhance both nucleation and growth rates as predicted by CNT. However, the temperature effects on nucleation rates become less important at lower temperatures (below 268 K), consistent with CLOUD studies (Duplissy et al., 2016) which found that sulfuric acid nucleation takes place at the kinetic limit without a Gibbs free energy barrier when temperature was low. These results emphasize the importance of NH_3 and other ternary species at warmer temperatures, for example, especially in the conditions present in the boundary layer.

Our results demonstrate that clusters formed at lower temperatures, while being transported to warmer temperatures, can survive evaporation and even grow further in the presence of SO_2 and ozone. We are providing the first this laboratory experimental evidence that support the mechanism of downward transport of newly formed particles from the free troposphere to the marine boundary layer proposed by several field and modelling studies (Russell et al., 1994;Raes, 1995;Clarke, 1993). Similarly, based on our results, it is reasonable to conclude that the new particles formed in the free troposphere over the Amazon forest are transferred downward to the warmer surface to act as a reservoir of nuclei mode particles (Wang et al., 2016), though the mechanism of growth is different from the one studied here (SO_2 + ozone).

Our results also show that the further growth is strongly dependent on the ozone level, implying that some unknown heterogeneous reaction processes involving SO_2 and ozone on sulfuric clusters may play important roles in NPF. These results can open a new research avenue for future studies for better understanding the roles of heterogeneous reactions involving nanoparticles and the effects of SO_2 on the nanoparticle growth. At present, it is not known why NPF takes place with high frequency and strong magnitude in extremely polluted megacities in China under the conditions with exceedingly high loadings of pre-existing aerosol particles (Guo et al., 2014;Yao et al., 2018;Yu et al., 2017b). The heterogeneous reactions involving SO_2 on nanoparticles proposed here, if they can be repeated and further understood in future studies, may provide some key insights into understanding the frequent nucleation and fast growth observed in these regions, where there are also very high concentrations of SO_2 and ozone.

Data Availability

All data of this work can be obtained from Lee Tiszenkel (lt0021@uah.edu) and Shanhu Lee (shanhu.lee@uah.edu).

Author Contributions

SL and MJ designed the experiments and LT, CS, JK, QO and MA carried them out. LT, QO and HY developed code used in the data analysis. LT, CS and QO performed the data analysis. LT and SL prepared the manuscript with contributions from all co-authors.

Competing interests

The authors declare that they have no conflict of interest.

Acknowledgements

This work was supported by NSF Awards AGS-1649719 and AGS-1649694. H. Yu acknowledges the support from the
National Key Research and Development Program of China (2016YFC0203100).

References

Almeida, J., Schobesberger, S., Kurten, A., Ortega, I. K., Kupiainen-Maatta, O., Praplan, A. P., Adamov, A., Amorim, A.,
Bianchi, F., Breitenlechner, M., David, A., Dommen, J., Donahue, N. M., Downard, A., Dunne, E., Duplissy, J., Ehrhart, S.,
Flagan, R. C., Franchin, A., Guida, R., Hakala, J., Hansel, A., Heinritzi, M., Henschel, H., Jokinen, T., Junninen, H., Kajos,
M., Kangasluoma, J., Keskinen, H., Kupc, A., Kurten, T., Kvashin, A. N., Laaksonen, A., Lehtipalo, K., Leiminger, M., Leppa,
J., Loukonen, V., Makhmutov, V., Mathot, S., McGrath, M. J., Nieminen, T., Olenius, T., Onnela, A., Petaja, T., Riccobono,
F., Riipinen, I., Rissanen, M., Rondo, L., Ruuskanen, T., Santos, F. D., Sarnela, N., Schallhart, S., Schnitzhofer, R., Seinfeld,
J. H., Simon, M., Sipila, M., Stozhkov, Y., Stratmann, F., Tome, A., Trostl, J., Tsagkogeorgas, G., Vaattovaara, P., Viisanen,
Y., Virtanen, A., Vrtala, A., Wagner, P. E., Weingartner, E., Wex, H., Williamson, C., Wimmer, D., Ye, P., Yli-Juuti, T.,
Carslaw, K. S., Kulmala, M., Curtius, J., Baltensperger, U., Worsnop, D. R., Vehkamaki, H., and Kirkby, J.: Molecular
understanding of sulphuric acid-amine particle nucleation in the atmosphere, Nature, 502, 359-363, 10.1038/nature12663,
2013.

Benson, D. R., Young, L. H., Kameel, R., and Lee, S. H.: Laboratory-measured sulfuric acid and water homogeneous
nucleation rates from the $SO_2 + OH$ reaction, Geophys. Res. Lett., 35, Doi:10.1029/2008GL033387, 10.1029/2008GL033387,
2008.

Benson, D. R., Erupe, M. E., and Lee, S. H.: Laboratory-measured H_2SO_4-H_2O-NH_3 ternary homogeneous nucleation rates:
initial observations Geophys. Res. Lett, 36, Doi:10.1029/2009GL038728, 10.1029/2009GL038728, 2009.

Benson, D. R., Al-Refai, M., and Lee, S.-H.: Chemical Ionization Mass Spectrometer (CIMS) for ambient measurments of
Ammonia, Atmos. Meas. Tech., 3, 1133-1162, 2010.

Benson, D. R., Yu, J. H., Markovich, A., and Lee, S. H.: Ternary homogeneous nucleation of H_2SO_4, NH_3, and H_2O under
conditions relevant to the lower troposphere, Atmospheric Chemistry and Physics, 11, 4755-4766, 10.5194/acp-11-4755-2011,
2011.

Berndt, T., Sipilä, M., Stratmann, F., Petäjä, T., Vanhanen, J., Mikkilä, J., Patokoski, J., Taipale, R., Mauldin III, R. L., and Kulmala, M.: Enhancement of atmospheric H_2SO_4 / H_2O nucleation: organic oxidation products versus amines, Atmos. Chem. Phys., 14, 751-764, 10.5194/acp-14-751-2014, 2014.

Brus, D., Hyvarinen, A. P., Viisanen, Y., Kulmala, M., and Lihavainen, H.: Homogenous nucleation of sulfuric acid and water mixture: experimental setup and first results, Atmos. Chem. Phys., 10, 2631-2641, 2010.

Chen, M., Titcombe, M., Jiang, J. K., Jen, C., Kuang, C. A., Fischer, M. L., Eisele, F. L., Siepmann, J. I., Hanson, D. R., Zhao, J., and McMurry, P. H.: Acid-base chemical reaction model for nucleation rates in the polluted atmospheric boundary layer, Proc. Natl. Acad. Sci. U. S. A., 109, 18713-18718, 10.1073/pnas.1210285109, 2012.

Clarke, A. D.: Atmospheric nuclei in the Pacific mid-troposphere: their nature, concentration, and evolution J. Geophys. Res., 98, 20633-20647, 1993.

Dunne, E. M., Gordon, H., Kürten, A., Almeida, J., Duplissy, J., Williamson, C., Ortega, I. K., Pringle, K. J., Adamov, A., Baltensperger, U., Barmet, P., Benduhn, F., Bianchi, F., Breitenlechner, M., Clarke, A., Curtius, J., Dommen, J., Donahue, N. M., Ehrhart, S., Flagan, R. C., Franchin, A., Guida, R., Hakala, J., Hansel, A., Heinritzi, M., Jokinen, T., Kangasluoma, J., Kirkby, J., Kulmala, M., Kupc, A., Lawler, M. J., Lehtipalo, K., Makhmutov, V., Mann, G., Mathot, S., Merikanto, J., Miettinen, P., Nenes, A., Onnela, A., Rap, A., Reddington, C. L. S., Riccobono, F., Richards, N. A. D., Rissanen, M. P., Rondo, L., Sarnela, N., Schobesberger, S., Sengupta, K., Simon, M., Sipilä, M., Smith, J. N., Stozhkov, Y., Tomé, A., Tröstl, J., Wagner, P. E., Wimmer, D., Winkler, P. M., Worsnop, D. R., and Carslaw, K. S.: Global atmospheric particle formation from CERN CLOUD measurements, Science, 354, 1119-1123, 2016.

Duplissy, J., Merikanto, J., Franchin, A., Tsagkogeorgas, G., Kangasluoma, J., Wimmer, D., Vuollekoski, H., Schobesberger, S., Lehtipalo, K., Flagan, R. C., Brus, D., Donahue, N. M., Vehkamäki, H., Almeida, J., Amorim, A., Barmet, P., Bianchi, F., Breitenlechner, M., Dunne, E. M., Guida, R., Henschel, H., Junninen, H., Kirkby, J., Kürten, A., Kupc, A., Määttänen, A., Makhmutov, V., Mathot, S., Nieminen, T., Onnela, A., Praplan, A. P., Riccobono, F., Rondo, L., Steiner, G., Tome, A., Walther, H., Baltensperger, U., Carslaw, K. S., Dommen, J., Hansel, A., Petäjä, T., Sipilä, M., Stratmann, F., Vrtala, A., Wagner, P. E., Worsnop, D. R., Curtius, J., and Kulmala, M.: Effect of ions on sulfuric acid-water binary particle formation: 2. Experimental data and comparison with QC-normalized classical nucleation theory, J. Geophys. Res., 121, 1752-1775, 10.1002/2015JD023539, 2016.

Eisele, F. L., and Tanner, D. J.: Measurements of gas phase concentrations of H_2SO_4 and methane sulfonic acid and estimates of H_2SO_4 production and loss in the atmosphere, J. Geophys. Res., 98, 9001-9010, 1993.

Erupe, M. E., Benson, D. R., Li, J., Young, L. H., Verheggen, B., Al-Refai, M., Tahboub, O., Cunningham, V., Frimpong, F., Viggiano, A. A., and Lee, S. H.: Correlation of aerosol nucleation rate with sulfuric acid and ammonia in Kent, Ohio: An atmospheric observation, J. Geophys. Res., 115, Doi:10.1029/2010JD013942, DOI:10.1029/2010JD013942, 2010.

Erupe, M. E., Viggiano, A. A., and Lee, S. H.: The effect of trimethylamine on atmospheric nucleation involving H_2SO_4, Atmos. Chem. Phys., 11, 4767-4775, 2011.

Frege, C., Ortega, I. K., Rissanen, M. P., Praplan, A. P., Steiner, G., Heinritzi, M., Ahonen, L., Amorim, A., Bernhammer, A. K., Bianchi, F., Brilke, S., Breitenlechner, M., Dada, L., Dias, A., Duplissy, J., Ehrhart, S., El-Haddad, I., Fischer, L., Fuchs, C., Garmash, O., Gonin, M., Hansel, A., Hoyle, C. R., Jokinen, T., Junninen, H., Kirkby, J., Kürten, A., Lehtipalo, K., Leiminger, M., Mauldin, R. L., Molteni, U., Nichman, L., Petäjä, T., Sarnela, N., Schobesberger, S., Simon, M., Sipilä, M., Stolzenburg, D., Tomé, A., Vogel, A. L., Wagner, A. C., Wagner, R., Xiao, M., Yan, C., Ye, P., Curtius, J., Donahue, N. M., Flagan, R. C., Kulmala, M., Worsnop, D. R., Winkler, P. M., Dommen, J., and Baltensperger, U.: Influence of temperature on the molecular composition of ions and charged clusters during pure biogenic nucleation, Atmos. Chem. Phys., 18, 65-79, 10.5194/acp-18-65-2018, 2018.

Glasoe, W. A., Volz, K., Panta, B., Freshour, N., Bachman, R., Hanson, D. R., McMurry, P. H., and Jen, C.: Sulfuric acid nucleation: an experimental study of the effect of seven bases, J. Geophys. Res., 120, 1933-1950, 10.1002/2014JD022730, 2015.

Gordon, H., Kirkby, J., Baltensperger, U., Bianchi, F., Breitenlechner, M., Curtius, J., Dias, A., Dommen, J., Donahue, N. M., Dunne, E. M., Duplissy, J., Ehrhart, S., Flagan, R. C., Frege, C., Fuchs, C., Hansel, A., Hoyle, C. R., Kulmala, M., Kurten, A., Lehtipalo, K., Makhmutov, V., Molteni, U., Rissanen, M. P., Stozhkov, Y., Trostl, J., Tsagkogeorgas, G., Wagner, R., Williamson, C., Wimmer, D., Winkler, P. M., Yan, C., and Carslaw, K. S.: Causes and importance of new particle formation in the present-day and preindustrial atmospheres, J. Geophys. Res.-Atmos., 122, 8739-8760, 10.1002/2017jd026844, 2017.

Guo, S., Hua, M., Zamor, M. L., Peng, J., Shang, D., Zheng, J., Du, Z., Wu, Z., Shao, M., Zeng, L., Molina, M. J., and Zhang, R.: Elucidating severe urban haze formation in China, Proc. Nat. Acad. Sci., 49, 17373–17378, 2014.

Hanson, D. R., and Eisele, F. L.: Diffusion of H_2SO_4 in humidified nitrogen: hydrated H_2SO_4, J. Phys. Chem., 104, 1715-1719, 2000.

Hanson, D. R., Bier, I., Panta, B., Jen, C. N., and McMurry, P. H.: Computational Fluid Dynamics Studies of a Flow Reactor: Free Energies of Clusters of Sulfuric Acid with NH_3 or Dimethyl Amine, J. Phys. Chem. A, 121, 3976-3990, 10.1021/acs.jpca.7b00252, 2017.

Hung, H.-M., and Hoffmann, M. R.: Oxidation of gas-phase SO_2 on the surfaces of acidic microdroplets: Implications for sulfate and sulfate radical anion formation in the atmospheric liquid phase, Environ. Sci. Technol., 49, 13768-13776, 2015.

Jen, C. N., McMurry, P. H., and Hanson, D. R.: Stabilization of sulfuric acid dimers by ammonia, methylamine, dimethylamine, and trimethylamine, J. Geophys. Res., 119, Doi: 10.1002/2014jd021592, 10.1002/2014jd021592, 2014.

Jen, C. N., Zhao, J., McMurry, P. H., and Hanson, D. R.: Chemical ionization of clusters formed from sulfuric acid and dimethylamine or diamines, Atmos. Chem. Phys., 16, 12513-12529, 10.5194/acp-16-12513-2016, 2016.

Kanawade, V. P., Guenther, A. B., Jobson, B. T., Erupe, M. E., Pressely, S. N., Tripathi, S. N., and Lee, S. H.: Isoprene suppression of new particle formation in a mixed decideous forest, Atmos. Chem. Phys., 11, 6013-6027, 2011.

Kashchiev, D.: On the relation between nucleation work, nucleus size, and nucleation rate, J. Phys. Chem., 76, 5098-5102, 10.1063/1.442808, 1982.

Khamaganov, V. G., and Hites, R. A.: Rate Constants for the Gas-Phase Reactions of Ozone with Isoprene, α- and β-Pinene, and Limonene as a Function of Temperature, The Journal of Physical Chemistry A, 105, 815-822, 10.1021/jp002730z, 2001.

Kirkby, J., Curtius, J., Almeida, J., Dunne, E., Duplissy, J., Ehrhart, S., Franchin, A., Gagne, S., Ickes, L., Kurten, A., Kupc, A., Metzger, A., Riccobono, F., Rondo, L., Schobesberger, S., Tsagkogeorgas, G., Wimmer, D., Amorim, A., Bianchi, F., Breitenlechner, M., David, A., Dommen, J., Downard, A., Ehn, M., Flagan, R. C., Haider, S., Hansel, A., Hauser, D., Jud, W., Junninen, H., Kreissl, F., Kvashin, A. N., Laaksonen, A., Lehtipalo, K., Lima, J., Lovejoy, E. R., Makhmutov, V., Mathot, S., Mikkila, J., Minginette, P., Mogo, S., Nieminen, T., Onnela, A., Pereira, P., Petaja, T., Schnitzhofer, R., Seinfeld, J. H., Sipila, M., Stozhkov, Y., Stratmann, F., Tome, A., Vanhanen, J., Viisanen, Y., Vrtala, A., Wagner, P. E., Walther, H., Weingartner, E., Wex, H., Winkler, P. M., Carslaw, K. S., Worsnop, D. R., Baltensperger, U., and Kulmala, M.: Role of sulphuric acid, ammonia and galactic cosmic rays in atmospheric aerosol nucleation, Nature, 476, 429-433, 2011.

Kirkby, J., Duplissy, J., Sengupta, K., Frege, C., Gordon, H., Williamson, C., Heinritzi, M., Simon, M., Yan, C., Almeida, J., Tröstl, J., Nieminen, T., Ortega, I. K., Wagner, R., Adamov, A., Amorim, A., Bernhammer, A.-K., Bianchi, F., Breitenlechner, M., Brilke, S., Chen, X., Craven, J., Dias, A., Ehrhart, S., Flagan, R. C., Franchin, A., Fuchs, C., Guida, R., Hakala, J., Hoyle, C. R., Jokinen, T., Junninen, H., Kangasluoma, J., Kim, J., Krapf, M., Kürten, A., Laaksonen, A., Lehtipalo, K., Makhmutov, V., Mathot, S., Molteni, U., Onnela, A., Peräkylä, O., Piel, F., Petäjä, T., Praplan, A. P., Pringle, K., Rap, A., Richards, N. A. D., Riipinen, I., Rissanen, M. P., Rondo, L., Sarnela, N., Schobesberger, S., Scott, C. E., Seinfeld, J. H., Sipilä, M., Steiner, G., Stozhkov, Y., Stratmann, F., Tomé, A., Virtanen, A., Vogel, A. L., Wagner, A. C., Wagner, P. E., Weingartner, E., Wimmer, D., Winkler, P. M., Ye, P., Zhang, X., Hansel, A., Dommen, J., Donahue, N. M., Worsnop, D. R., Baltensperger, U., Kulmala, M., Carslaw, K. S., and Curtius, J.: Ion-induced nucleation of pure biogenic particles, Nature, 533, 521-526, 10.1038/nature17953, 2016.

Krasnomowitz, J. M., Apsokardu, M. J., Stangl, C. M., Tiszenkel, L., Ouyang, Q., Lee, S., and Johnston, M. V.: Growth of Aitken mode ammonium sulfate particles by α-pinene ozonolysis, Aerosol Science and Technology, 53, 406-418, 10.1080/02786826.2019.1568381, 2019.

Kulmala, M., Kontkanen, J., Junninen, H., Lehtipalo, K., Manninen, H. E., Nieminen, T., Petäjä, T., Sipilä, M., Schobesberger, S., Rantala, P., Franchin, A., Jokinen, T., Järvinen, E., Äijälä, M., Kangasluoma, J., Hakala, J., Aalto, P. P., Paasonen, P., Mikkilä, J., Vanhanen, J., Aalto, J., Hakola, H., Makkonen, U., Ruuskanen, T., Mauldin, R. L., Duplissy, J., Vehkamäki, H., Bäck, J., Kortelainen, A., Riipinen, I., Kurtén, T., Johnston, M. V., Smith, J. N., Ehn, M., Mentel, T. F., Lehtinen, K. E. J., Laaksonen, A., Kerminen, V. M., and Worsnop, D. R.: Direct observations of atmospheric aerosol nucleation, Science, 339, 943-946, 10.1126/science.1227385, 2013.

Kulmala, M., Kerminen, V.-M., Petaja, T., Ding, A., and Wang, L.: Atmospheric gas-to-particle conversion: why NPF events are observed in megacities?, Faraday Discussions, Doi: 10.1039/C1036FD00257A, 10.1039/c6fd00257a, 2017.

Kürten, A., Rondo, L., Ehrhart, S., and Curtius, J.: Calibration of a chemical ionization mass spectrometer for the measurement of gaseous sulfuric acid, The Journal of Physical Chemistry A, 116, 6375-6386, 10.1021/jp212123n, 2012.

Kürten, A., Jokinen, T., Simon, M., Sipilä, M., Sarnela, N., Junninen, H., Adamov, A., Almeida, J., Amorim, A., Bianchi, F., Breitenlechner, M., Dommen, J., Donahue, N. M., Duplissy, J., Ehrhart, S., Flagan, R. C., Franchin, A., Hakala, J., Hansel, A., Heinritzi, M., Hutterli, M., Kangasluoma, J., Kirkby, J., Laaksonen, A., Lehtipalo, K., Leiminger, M., Makhmutov, V., Mathot, S., Onnela, A., Petäjä, T., Praplan, A. P., Riccobono, F., Rissanen, M. P., Rondo, L., Schobesberger, S., Seinfeld, J. H., Steiner, G., Tomé, A., Tröstl, J., Winkler, P. M., Williamson, C., Wimmer, D., Ye, P., Baltensperger, U., Carslaw, K. S., Kulmala, M., Worsnop, D. R., and Curtius, J.: Neutral molecular cluster formation of sulfuric acid–dimethylamine observed in real time under atmospheric conditions, Proc. Nat. Acad. Sci., 111, 15019-15024, 10.1073/pnas.1404853111, 2014.

Kürten, A., Bianchi, F., Almeida, J., Kupiainen-Määttä, O., Dunne, E. M., Duplissy, J., Williamson, C., Barmet, P., Breitenlechner, M., Dommen, J., Donahue, N. M., Flagan, R. C., Franchin, A., Gordon, H., Hakala, J., Hansel, A., Heinritzi, M., Ickes, L., Jokinen, T., Kangasluoma, J., Kim, J., Kirkby, J., Kupc, A., Lehtipalo, K., Leiminger, M., Makhmutov, V., Onnela, A., Ortega, I. K., Petäjä, T., Praplan, A. P., Riccobono, F., Rissanen, M. P., Rondo, L., Schnitzhofer, R., Schobesberger, S., Smith, J. N., Steiner, G., Stozhkov, Y., Tomé, A., Tröstl, J., Tsagkogeorgas, G., Wagner, P. E., Wimmer, D., Ye, P., Baltensperger, U., Carslaw, K., Kulmala, M., and Curtius, J.: Experimental particle formation rates spanning tropospheric sulfuric acid and ammonia abundances, ion production rates, and temperatures, J. Geophys. Res., 121, 12377-12400, 10.1002/2015JD023908, 2016.

Lee, S.-H., Uin, J., Guenther, A. B., Gouw, J. A. d., Yu, F., Nadykto, A. B., Herb, J., Ng, N. L., Koss, A., Brune, W. H., Baumann, K., Kanawad, V. P., Keutsch, F. N., Nenes, A., Olsen, K., Goldstein, A., and Qi, O.: Isoprene suppression of new particle formation: Potential mechanism and implications, J. Geophys. Res., 121, Doi:10.1029/2016JD024844 10.1029/2016JD024844 2016.

Lehtipalo, K., Leppä, J., Kontkanen, J., Kangasluoma, J., Franchin, A., Wimmer, D., Schobesberger, S., Junninen, H., Petäjä, T., Sipilä, M., Mikkilä, J., Vanhanen, J., Worsnop, D. R., and Kulmala1, M.: Methods for determining particle size distribution and growth rates between 1 and 3 nm using the Particle Size Magnifier, Boreal Environ. Res., 19, 215–236, 2014.

Lehtipalo, K., Rondo, L., Kontkanen, J., Schobesberger, S., Jokinen, T., Sarnela, N., Kürten, A., Ehrhart, S., Franchin, A., Nieminen, T., Riccobono, F., Sipilä, M., Yli-Juuti, T., Duplissy, J., Adamov, A., Ahlm, L., Almeida, J., Amorim, A., Bianchi, F., Breitenlechner, M., Dommen, J., Downard, A. J., Dunne, E. M., Flagan, R. C., Guida, R., Hakala, J., Hansel, A., Jud, W., Kangasluoma, J., Kerminen, V.-M., Keskinen, H., Kim, J., Kirkby, J., Kupc, A., Kupiainen-Määttä, O., Laaksonen, A., Lawler, M. J., Leiminger, M., Mathot, S., Olenius, T., Ortega, I. K., Onnela, A., Petäjä, T., Praplan, A., Rissanen, M. P., Ruuskanen, T., Santos, F. D., Schallhart, S., Schnitzhofer, R., Simon, M., Smith, J. N., Tröstl, J., Tsagkogeorgas, G., Tomé, A., Vaattovaara, P., Vehkamäki, H., Vrtala, A. E., Wagner, P. E., Williamson, C., Wimmer, D., Winkler, P. M., Virtanen, A., Donahue, N. M., Carslaw, K. S., Baltensperger, U., Riipinen, I., Curtius, J., Worsnop, D. R., and Kulmala, M.: The effect of acid–base clustering and ions on the growth of atmospheric nano-particles, Nat. Commun., 7, 11594, 10.1038/ncomms11594, 2016.

Lehtipalo, K., Yan, C., Dada, L., Bianchi, F., Xiao, M., Wagner, R., Stolzenburg, D., Ahonen, L. R., Amorim, A., Baccarini, A., Bauer, P. S., Baumgartner, B., Bergen, A., Bernhammer, A.-K., Breitenlechner, M., Brilke, S., Buchholz, A., Mazon, S.

B., Chen, D., Chen, X., Dias, A., Dommen, J., Draper, D. C., Duplissy, J., Ehn, M., Finkenzeller, H., Fischer, L., Frege, C., Fuchs, C., Garmash, O., Gordon, H., Hakala, J., He, X., Heikkinen, L., Heinritzi, M., Helm, J. C., Hofbauer, V., Hoyle, C. R., Jokinen, T., Kangasluoma, J., Kerminen, V.-M., Kim, C., Kirkby, J., Kontkanen, J., Kürten, A., Lawler, M. J., Mai, H., Mathot, S., Mauldin, R. L., Molteni, U., Nichman, L., Nie, W., Nieminen, T., Ojdanic, A., Onnela, A., Passananti, M., Petäjä, T., Piel, F., Pospisilova, V., Quéléver, L. L. J., Rissanen, M. P., Rose, C., Sarnela, N., Schallhart, S., Schuchmann, S., Sengupta, K., Simon, M., Sipilä, M., Tauber, C., Tomé, A., Tröstl, J., Väisänen, O., Vogel, A. L., Volkamer, R., Wagner, A. C., Wang, M., Weitz, L., Wimmer, D., Ye, P., Ylisirniö, A., Zha, Q., Carslaw, K. S., Curtius, J., Donahue, N. M., Flagan, R. C., Hansel, A., Riipinen, I., Virtanen, A., Winkler, P. M., Baltensperger, U., Kulmala, M., and Worsnop, D. R.: Multicomponent new particle formation from sulfuric acid, ammonia, and biogenic vapors, 4, eaau5363, 10.1126/sciadv.aau5363 %J Science Advances, 2018.

Lovejoy, E. R., Curtius, J., and Froyd, K. D.: Atmospheric ion-induced nucleation of sulfuric acid and water J. Geophys. Res., 109, Doi: 10.1029/2003JD004460, 10.1029/2003JD004460, 2004.

Malila, J., McGraw, R., Laaksonen, A., and Lehtinen, K. E. J.: Repairing the first nucleation theorem: Precritical cluster losses, 1527, 31-34, 10.1063/1.4803197, 2013.

Martin, S. T., Artaxo, P., Machado, L., Manzi, A. O., Souza, R. A. F., Schumacher, C., Wang, J., Biscaro, T., Brito, J., Calheiros, A., Jardine, K., Medeiros, A., Portela, B., de Sá, S. S., Adachi, K., Aiken, A. C., Albrecht, R., Alexander, L., Andreae, M. O., Barbosa, H. M. J., Buseck, P., Chand, D., Comstock, J. M., Day, D. A., Dubey, M., Fan, J., Fast, J., Fisch, G., Fortner, E., Giangrande, S., Gilles, M., Goldstein, A. H., Guenther, A., Hubbe, J., Jensen, M., Jimenez, J. L., Keutsch, F. N., Kim, S., Kuang, C., Laskin, A., McKinney, K., Mei, F., Miller, M., Nascimento, R., Pauliquevis, T., Pekour, M., Peres, J., Petäjä, T., Pöhlker, C., Pöschl, U., Rizzo, L., Schmid, B., Shilling, J. E., Dias, M. A. S., Smith, J. N., Tomlinson, J. M., Tóta, J., and Wendisch, M.: The Green Ocean Amazon Experiment (GoAmazon2014/5) Observes Pollution Affecting Gases, Aerosols, Clouds, and Rainfall over the Rain Forest, Bulletin of the American Meteorological Society, 98, 981-997, 10.1175/BAMS-D-15-00221.1, 2016.

McGraw, R., and Zhang, R.: Multivariate analysis of homogeneous nucleation rate measurements. Nucleation in the p-toluic acid/sulfuric acid/water system, J. Chem. Phys., 128, Doi: 10.1063/1061.2830030, 10.1063/1.2830030, 2008.

Merikanto, J., Spracklen, D. V., Mann, G. W., Pickering, S. J., and Carslaw, K. S.: Impact of nucleation on global CCN, Atmos. Chem. Phys., 9, 8601-8616, 2009.

Nieminen, T., Paasonen, P., Manninen, H. E., Sellegri, K., Kerminen, V. M., and Kulmala, M.: Parameterization of ion-induced nucleation rates based on ambient observations, Atmos. Chem. Phys., 11, 3393-3402, 10.5194/acp-11-3393-2011, 2011.

Petäjä, T., Mauldin III, R. L., Kosciuch, E., McGrath, J., Nieminen, T., Paasonen, P., Boy, M., Adamov, A., Kotiaho, T., and Kulmala, M.: Sulfuric acid on OH concentrations in boreal forest site, Atmos. Chem. Phys., 9, 7435-7448, 2009.

Raes, F.: Entrainment of free tropospheric aerosols as a regulating mechanism for cloud condensation nuclei in the remote marine boundary layer, 100, 2893-2903, 10.1029/94jd02832, 1995.

Rizzo, V. L., Roldin, P., Brito, J., Backman, J., Swietlicki, E., Krejci, R., Tunved, P., Petäjä, T., Kulmala, M., and Artaxo, P.: Multi-year statistical and modeling analysis of submicrometer aerosol number size distributions at a rain forest site in Amazonia, Atmos. Chem. Phys., 18, 10255-10274, 10.5194/acp-18-10255-2018, 2018.

Russell, L. M., Pandis, S. N., and Seinfeld, J. H.: Aerosol production and growth in the marine boundary layer, Journal of Geophysical Research: Atmospheres, 99, 20989-21003, 10.1029/94jd01932, 1994.

Schobesberger, S., Franchin, A., Bianchi, F., Rondo, L., Duplissy, J., Kürten, A., Ortega, I. K., Metzger, A., Schnitzhofer, R., Almeida, J., Amorim, A., Dommen, J., Dunne, E. M., Ehn, M., Gagné, S., Ickes, L., Junninen, H., Hansel, A., Kerminen, V. M., Kirkby, J., Kupc, A., Laaksonen, A., Lehtipalo, K., Mathot, S., Onnela, A., Petäjä, T., Riccobono, F., Santos, F. D., Sipilä, M., Tomé, A., Tsagkogeorgas, G., Viisanen, Y., Wagner, P. E., Wimmer, D., Curtius, J., Donahue, N. M., Baltensperger, U., Kulmala, M., and Worsnop, D. R.: On the composition of ammonia–sulfuric-acid ion clusters during aerosol particle formation, Atmos. Chem. Phys., 15, 55-78, 10.5194/acp-15-55-2015, 2015.

Seinfeld, J. H., and Pandis, S. N.: Atmospheric chemistry and physics: From air pollution to climate change, John Wiley and Sons, Inc., New Jersey, 2016.

Skrabalova, L., Brus, D., Anttila, T., Zdimal, V., and Lihavainen, H.: Growth of sulphuric acid nanoparticles under wet and dry conditions, Atmos. Chem. Phys., 14, 6461-6475, 10.5194/acp-14-6461-2014, 2014.

Stangl, C. M., Krasnomowitz, J. M., Apsokardu, M. J., Tiszenkel, L., Ouyang, Q., Lee, S., and Johnston, M. V.: Sulfur Dioxide Modifies Aerosol Particle Formation and Growth by Ozonolysis of Monoterpenes and Isoprene, 124, 4800-4811, 10.1029/2018jd030064, 2019.

Stolzenburg, D., Fischer, L., Vogel, A. L., Heinritzi, M., Schervish, M., Simon, M., Wagner, A. C., Dada, L., Ahonen, L. R., Amorim, A., Baccarini, A., Bauer, P. S., Baumgartner, B., Bergen, A., Bianchi, F., Breitenlechner, M., Brilke, S., Mazon, S. B., Chen, D. X., Dias, A., Draper, D. C., Duplissy, J., Haddad, I., Finkenzeller, H., Frege, C., Fuchs, C., Garmash, O., Gordon, H., He, X., Helm, J., Hofbauer, V., Hoyle, C. R., Kim, C., Kirkby, J., Kontkanen, J., Kuerten, A., Lampilahti, J., Lawler, M., Lehtipalo, K., Leiminger, M., Mai, H., Mathot, S., Mentler, B., Molteni, U., Nie, W., Nieminen, T., Nowak, J. B., Ojdanic, A., Onnela, A., Passananti, M., Petaja, T., Quelever, L. L. J., Rissanen, M. P., Sarnela, N., Schallhart, S., Tauber, C., Tome, A., Wagner, R., Wang, M., Weitz, L., Wimmer, D., Xiao, M., Yan, C., Ye, P., Zha, Q., Baltensperger, U., Curtius, J., Dommen, J., Flagan, R. C., Kulmala, M., Smith, J. N., Worsnop, D. R., Hansel, A., Donahue, N. M., and Winkler, P. M.: Rapid growth of organic aerosol nanoparticles over a wide tropospheric temperature range, Proc. Natl. Acad. Sci. U. S. A., 115, 9122-9127, 10.1073/pnas.1807604115, 2018.

Tröstl, J., Chuang, W. K., Gordon, H., Heinritzi, M., Yan, C., Molteni, U., Ahlm, L., Frege, C., Bianchi, F., Wagner, R., Simon, M., Lehtipalo, K., Williamson, C., Craven, J. S., Duplissy, J., Adamov, A., Almeida, J., Bernhammer, A.-K., Breitenlechner, M., Brilke, S., Dias, A., Ehrhart, S., Flagan, R. C., Franchin, A., Fuchs, C., Guida, R., Gysel, M., Hansel, A., Hoyle, C. R., Jokinen, T., Junninen, H., Kangasluoma, J., Keskinen, H., Kim, J., Krapf, M., Kürten, A., Laaksonen, A., Lawler, M., Leiminger, M., Mathot, S., Möhler, O., Nieminen, T., Onnela, A., Petäjä, T., Piel, F. M., Miettinen, P., Rissanen, M. P., Rondo, L., Sarnela, N., Schobesberger, S., Sengupta, K., Sipilä, M., Smith, J. N., Steiner, G., Tomè, A., Virtanen, A., Wagner, A. C.,

Weingartner, E., Wimmer, D., Winkler, P. M., Ye, P., Carslaw, K. S., Curtius, J., Dommen, J., Kirkby, J., Kulmala, M., Riipinen, I., Worsnop, D. R., Donahue, N. M., and Baltensperger, U.: The role of low-volatility organic compounds in initial particle growth in the atmosphere, Nature, 533, 527-531, 10.1038/nature18271, 2016.

Vanhanen, J., Mikkila, J., Lehtipalo, K., Sipila, M., Manninen, H. E., Siivola, E., Petaja, T., and Kulmala, M.: Particle size magnifier for nano-CN detection, Aerosol Sci. Technol., 45, 533-542, 10.1080/02786826.2010.547889, 2011.

Vehkamäki, H., McGrath, M. J., Kurtén, T., Julin, J., Lehtinen, K. E. J., and Kulmala, M.: Rethinking the application of the first nucleation theorem to particle formation, J. Chem. Phys., 136, Doi: 10.1063/1061.3689227, 2012.

Wang, J., Krejci, R., Giangrande, S., Kuang, C., Barbosa, H. M. J., Brito, J., Carbone, S., Chi, X., Comstock, J., Ditas, F., Lavric, J., Manninen, H. E., Mei, F., Moran-Zuloaga, D., Pöhlker, C., Pöhlker, M. L., Saturno, J., Schmid, B., Souza, R. A. F., Springston, S. R., Tomlinson, J. M., Toto, T., Walter, D., Wimmer, D., Smith, J. N., Kulmala, M., Machado, L. A. T., Artaxo, P., Andreae, M. O., Petäjä, T., and Martin, S. T.: Amazon boundary layer aerosol concentration sustained by vertical transport during rainfall, Nature, 539, 416-419, 10.1038/nature19819, 2016.

Wang, M., and Penner, J. E.: Aerosol indirect forcing in a global model with particle nucleation, Atmos. Chem. Phys., 9, 239-260, 2009.

Yao, L., Garmash, O., Bianchi, F., Zheng, J., Yan, C., Kontkanen, J., Junninen, H., Mazon, S. B., Ehn, M., Paasonen, P., Sipila, M., Wang, M. Y., Wang, X. K., Xiao, S., Chen, H. F., Lu, Y. Q., Zhang, B. W., Wang, D. F., Fu, Q. Y., Geng, F. H., Li, L., Wang, H. L., Qiao, L. P., Yang, X., Chen, J. M., Kerminen, V. M., Petaja, T., Worsnop, D. R., Kulmala, M., and Wang, L.: Atmospheric new particle formation from sulfuric acid and amines in a Chinese megacity, Science, 361, 278-281, 10.1126/science.aao4839, 2018.

You, Y., Kanawade, V. P., de Gouw, J. A., Guenther, A. B., Madronich, S., Sierra-Hernández, M. R., Lawler, M., Smith, J. N., Takahama, S., Ruggeri, G., Koss, A., Olson, K., Baumann, K., Weber, R. J., Nenes, A., Guo, H., Edgerton, E. S., Porcelli, L., Brune, W. H., Goldstein, A. H., and Lee, S. H.: Atmospheric amines and ammonia measured with a Chemical Ionization Mass Spectrometer (CIMS), Atmos. Chem. Phys. , 14, 12181-12194, 10.5194/acpd-14-16411-2014, 2014.

Young, L. H., Benson, D. R., Rifkha, F., Pierce, J. R., Junninen, H., Kulmala, M., and Lee, S. H.: Laboratory studies of sulfuric acid and water binary homogeneous nucleation: evaluation of laboratory setup and preliminary results, Atmos. Chem. Phys., 8, 1-20, 2008a.

Young, L. H., Benson, D. R., Rifkha, F., Pierce, J. R., Junninen, H., Kulmala, M., and Lee, S. H.: Laboratory studies of sulfuric acid and water binary homogeneous nucleation: Evaluation of laboratory setup and preliminary results, Atmos. Chem. Phys., 8, 4997-5016, 2008b.

Yu, F., and Luo, G.: Simulation of particle size distribution with a global aerosol model: contribution of nucleation to aerosol and CCN number concentrations, Atmos. Chem. Phys., 9, 7691-7710, 10.5194/acp-9-7691-2009, 2009.

Yu, F., Luo, G., Pryor, S. C., Pillai, P. R., Lee, S. H., Ortega, J., Schwab, J. J., Hallar, A. G., Leaitch, W. R., Aneja, V. P., Smith, J. N., Walker, J. T., Hogrefe, O., and Demerjian, K. L.: Spring and summer contrast in new particle formation over nine forest areas in North America, Atmos. Chem. Phys., 15, 13993-14003, 10.5194/acpd-15-21271-2015, 2015.

Yu, H., McGraw, R., and Lee, S. H.: Effects of amines on formation of sub-3 nm particles and their subsequent growth, Geophys. Res. Lett., 39, Doi: 10.1029/2011gl050099, 10.1029/2011gl050099, 2012.

Yu, H., and Lee, S. H.: A chemical ionization mass spectrometer for the detection of atmospheric amines, Environ. Chem., 9, 190-201, 2012

5 Yu, H., Dai, L., Zhao, Y., Kanawade, V. P., Tripathi, S. N., Ge, X., Chen, M., and Lee, S.-H.: Laboratory observations of temperature and humidity dependencies of nucleation and growth rates of sub-3 nm particles, J. Geophys. Res., 122, 1919-1929, 10.1002/2016JD025619, 2017a.

Yu, H., Ren, L., and Kanawade, V. P.: New Particle Formation and Growth Mechanisms in Highly Polluted Environments, Current Pollution Reports, 3, 245-253, 10.1007/s40726-017-0067-3, 2017b.

10 Zhang, R., Khalizov, A. F., Wang, L., Hu, M., and Xu, W.: Nucleation and growth of nanoparticles in the atmosphere, Chem. Rev., 112, 957-2011, 2012.

Zollner, J. H., Glasoe, W. A., Panta, B., Carlson, K. K., McMurry, P. H., and Hanson, D. R.: Sulfuric acid nucleation: power dependencies, variation with relative humidity, and effect of bases, Atmos. Chem. Phys., 12, 4399-4411, 10.5194/acp-12-4399-2012, 2012.

Table 1. Typical experimental conditions used in FT-1 and FT-2. *J* in FT-1 is the nucleation rate for sub-2 nm particles. *J* in FT-2 is the formation rate of total particles in the size range from 3 to 60 nm; the particle mean diameter ranged from 2.7 to 3.4 nm depending on the ozone concentration. *GR* in FT-1 is the growth rate of sub-3 nm particles. *GR* in FT-2 is the growth rate of total particles from 3 to 60 nm.

FT-1: Nucleation Region						FT-2: Growth Region	
Temperature (K)	297	288	278	268	258	Temperature (K)	297
RH	20% - 45%	8% - 60%	12% - 80%	23% - 80%	46% - 85%	RH	10%
$[H_2SO_4]$ (cm^{-3})	$1\times10^7 - 3\times10^8$	$7\times10^6 - 2\times10^8$	$2\times10^6 - 7\times10^7$	$2\times10^6 - 4\times10^7$	$4\times10^6 - 7\times10^7$	SO_2 (ppbv)	100-5000
RA	$4\times10^{-5} - 7\times10^{-4}$	$7\times10^{-5} - 1\times10^{-3}$	$6\times10^{-5} - 2\times10^{-3}$	$3\times10^{-4} - 5\times10^{-3}$	$3\times10^{-3} - 4\times10^{-2}$	O_3 (ppbv)	0 - 248
GR $(nm\ h^{-1})$	1 - 20	1 - 20	2 - 80	3 - 45	2 – 35	GR $(nm\ h^{-1})$	12.0- 28.1
J $(cm^{-3}\ s^{-1})$	$10^1 – 10^5$	$10^2 – 10^5$	$10^2 – 10^5$	$10^2 – 10^5$	$10^2 – 10^5$	J $(cm^{-3}\ s^{-1})$	0 - 189.9
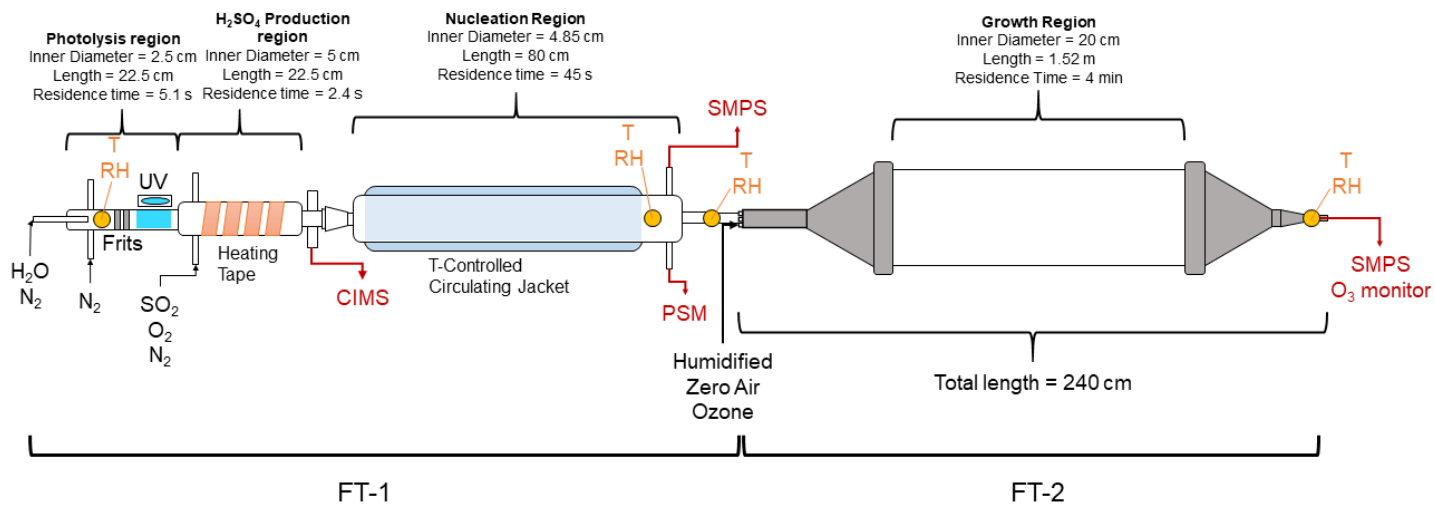
Figure 1. Schematic diagram of the TANGENT experimental setup. This setup consists of two flow tubes (FT). T indicates temperature. FT-1 is used as the nucleation region and FT-2 as the growth region. Table 1 shows the typical experimental conditions used during the 2018 IOP study.
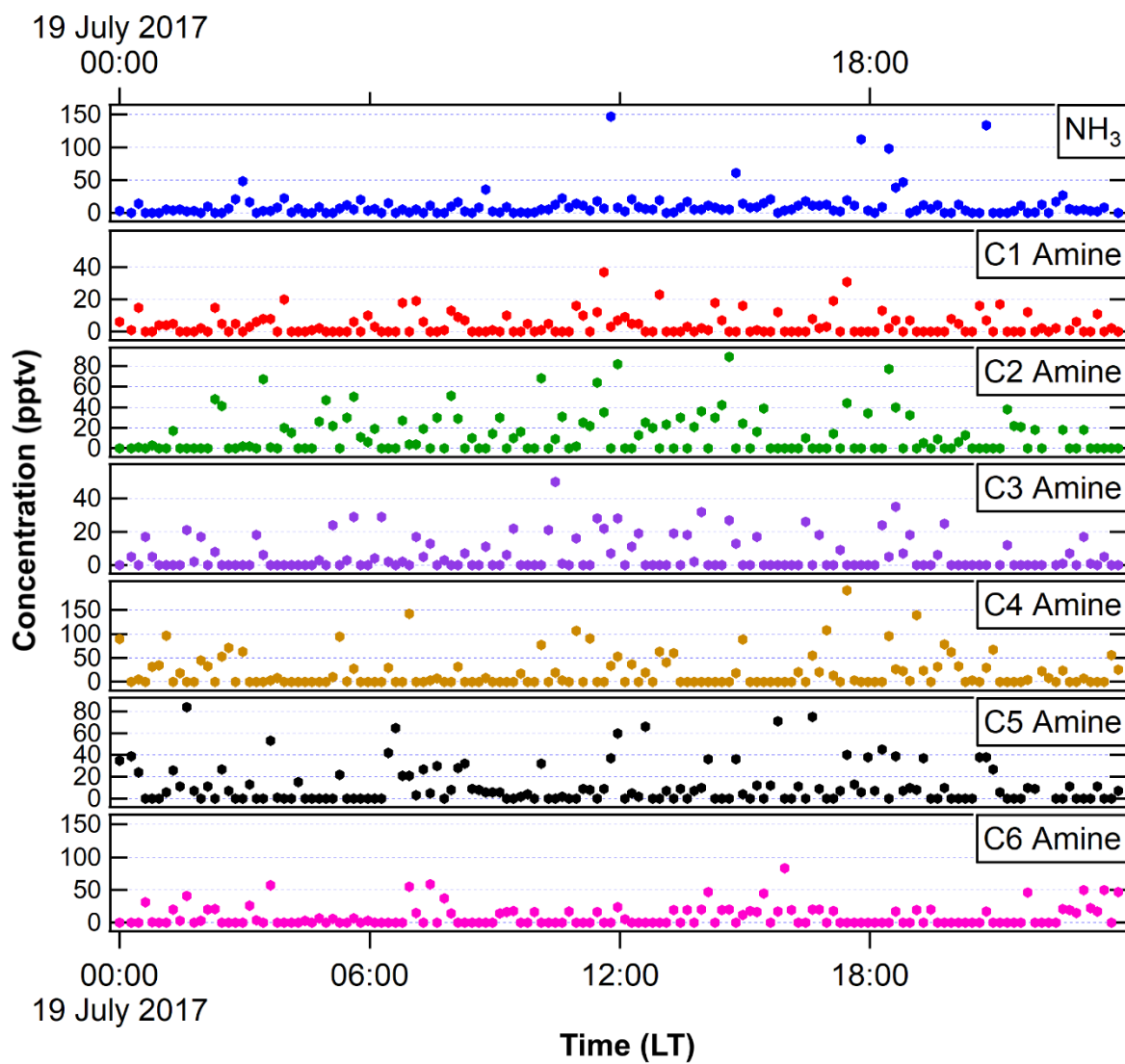
Figure 2. NH₃ and amines measured with the ethanol-CIMS in the FT-1 during the 2017 IOP in a very similar experimental condition as in 2018 IOP. We show here as an example one day of measurements (July 19, 2017).
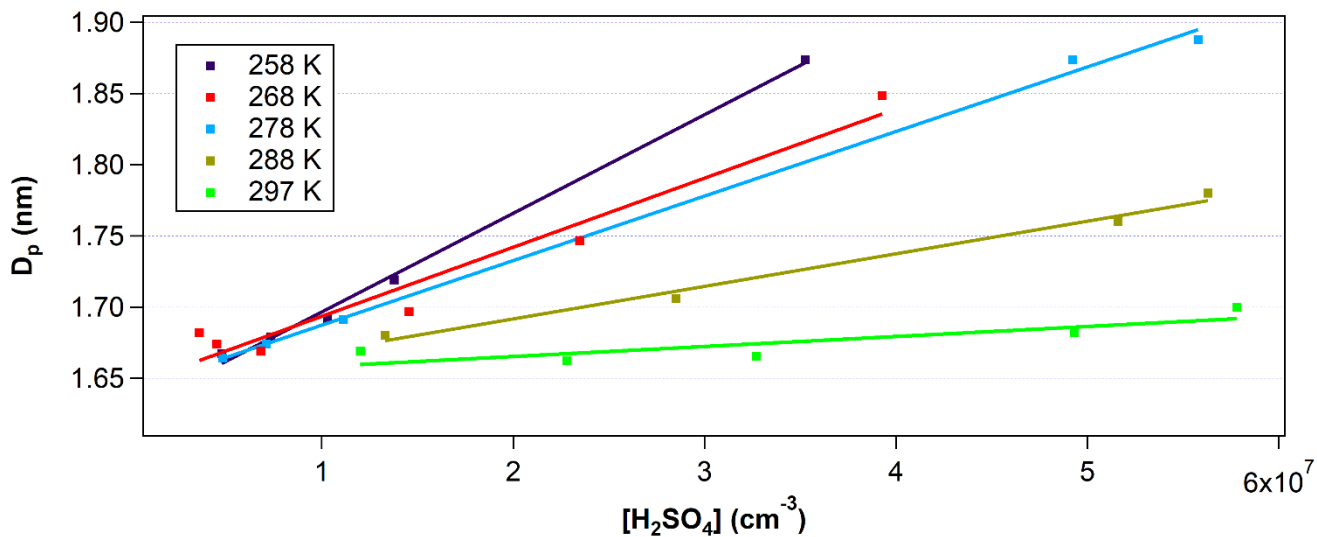
Figure 3. Mean diameter of particles (D_p) inverted from the PSM measurements at the end of the nucleation tube as a function of [H_2SO_4] and temperature. Data points were taken at RH between 20% and 30%. Solid lines are linear fittings of the measurement data (coloured squares) under different temperatures. Error in [H_2SO_4] is estimated to be ±60%. Error in D_p at this size range is estimated to be ±0.2 nm, or approximately ±12%.
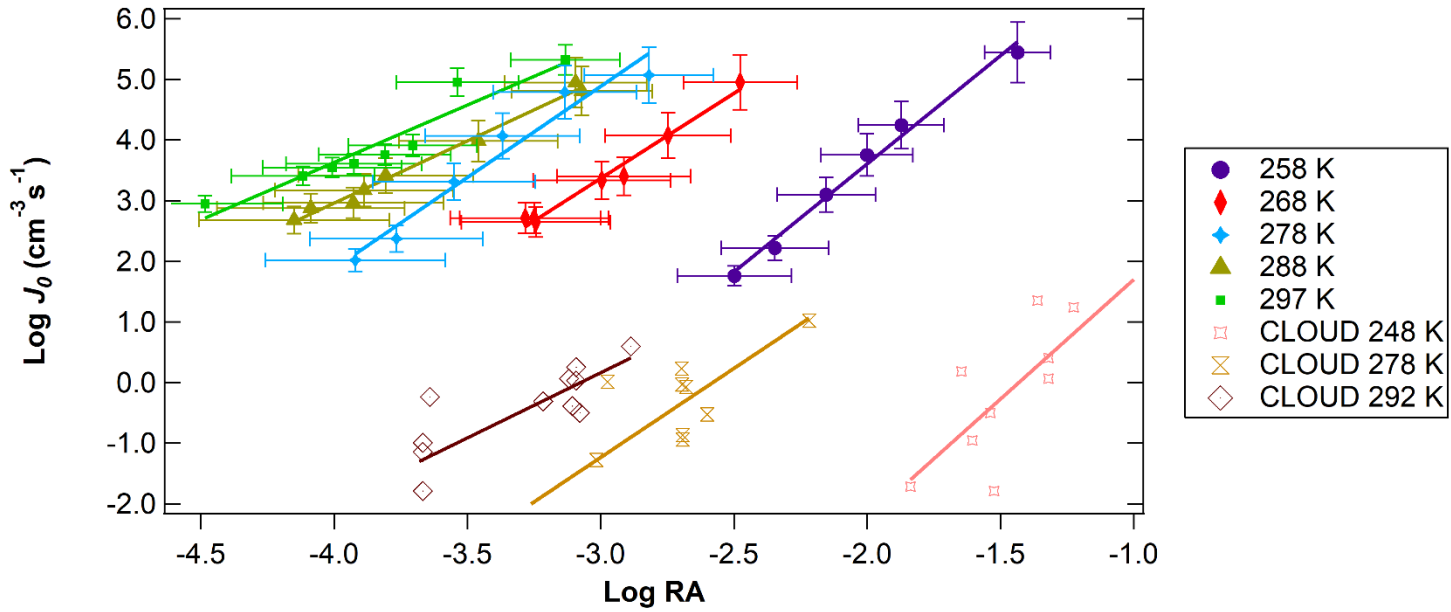
Figure 4. Log J_0 vs. Log RA for different temperatures at a relatively constant RH (41% - 45%). Temperatures ranged from 258 to 297 K. CLOUD data for similar RA and temperature conditions is shown from (Dunne et al., 2016)
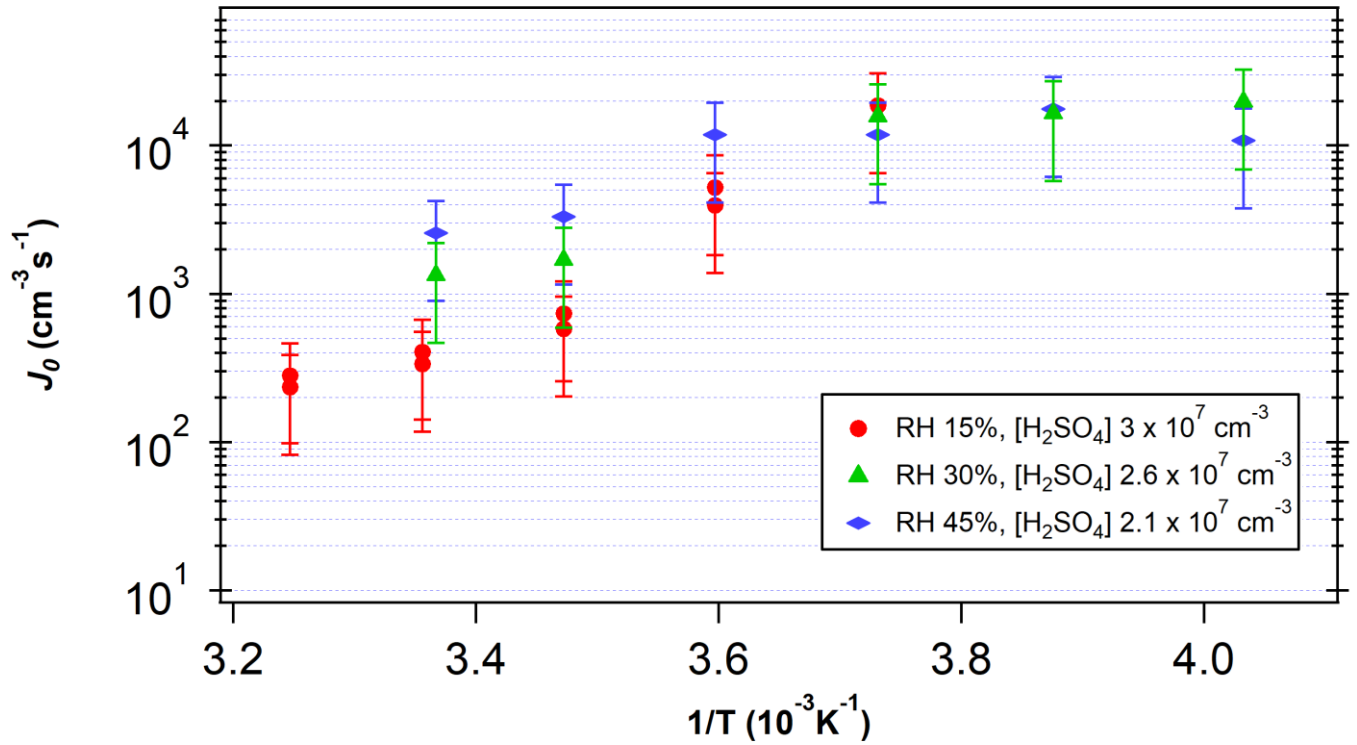
Figure 5. Log J_0 vs. 1/T for [H$_2$SO$_4$] between 2×10^7 and 3×10^7 cm^{-3}. T is the temperature in FT-1. RH ranged from 15% to 45%. Vertical bars indicate one standard deviation of the measured nucleation rates.
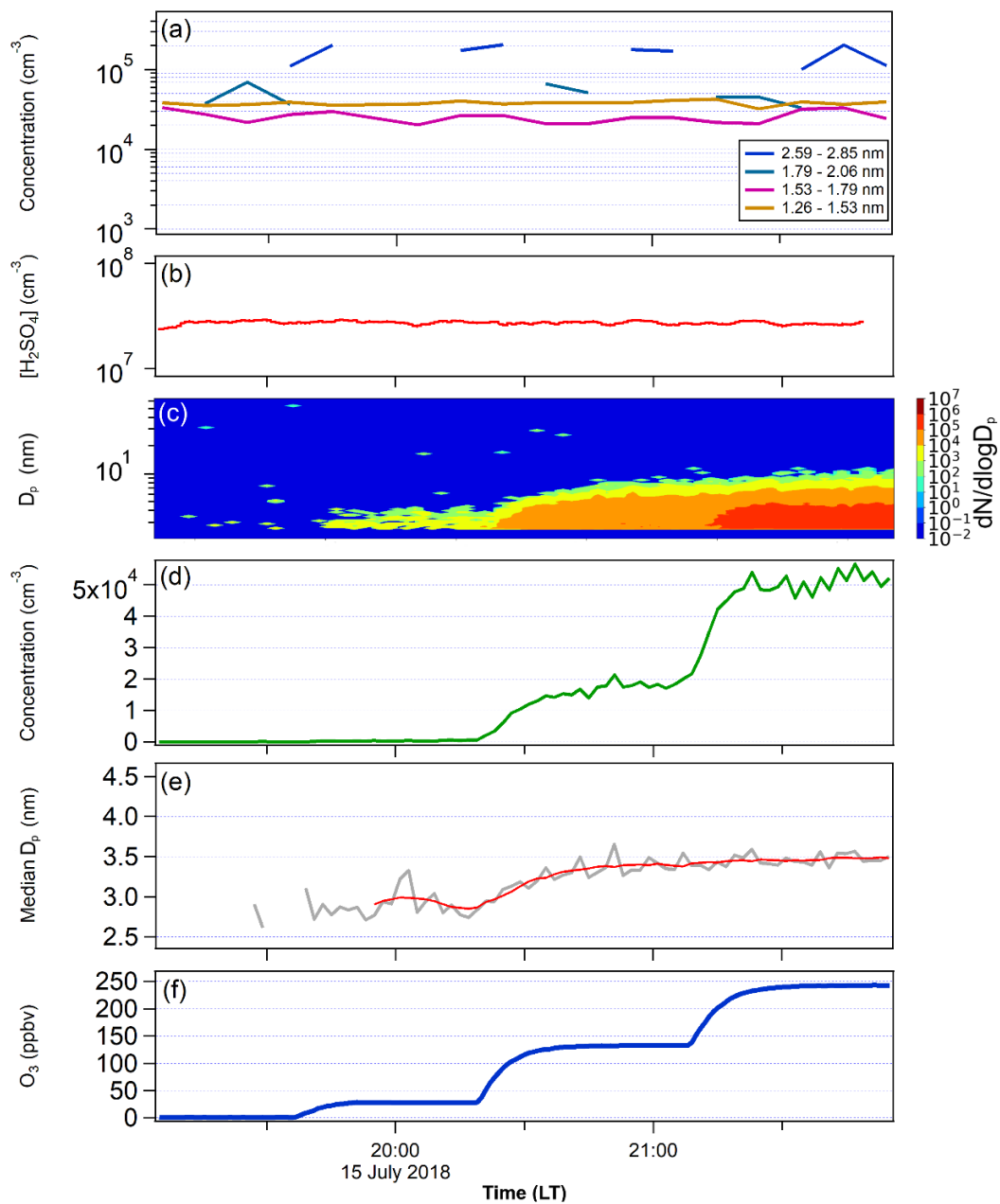
Figure 6. (a) The PSM-inverted size distribution and (b) [H_2SO_4] measured in FT-1 during the temperature gradient TANGENT experiment.FT-1 was at 268 K, residence time 45 s. Total concentration at the end of FT-1 was 1.79×10^5 cm^{-3} with a mean D_p of 1.9 nm. (c) SMPS-measured particle size distribution, (d) total number concentration, (e) the particle median diameter D_p, and (f) Ozone concentrations in FT-2. FT-2 was kept at 297 K, and the residence time was 4 min. The red line in (e) indicates the average values of D_p. SO$_2$ was 500 and 83 ppbv in FT-1 and FT-2, respectively. H$_2$SO$_4$ was not measured at FT-2; however, after considering wall loss in FT-1 and the 1:6 dilution FT-2, [H_2SO_4] in FT-2 was estimated to be 1.15×10^6 cm^{-3}.
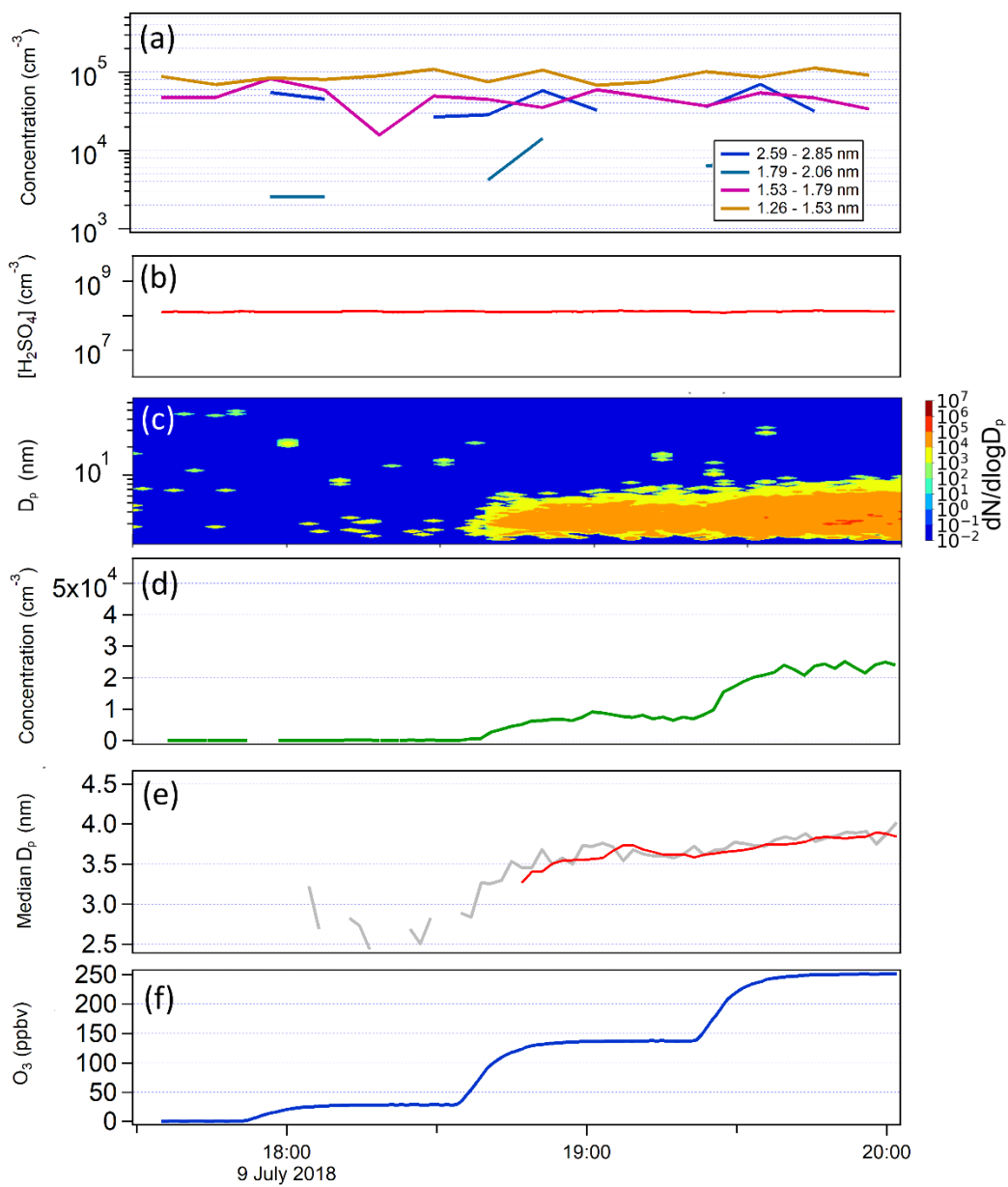
Figure 7. The same as Figure 6, except that FT-1 and FT-2 had the same temperature in this test. Total particle concentration at the end of FT-1 was 1.7×10^5 cm^{-3} with a mean D_p of 1.9 nm and [H$_2$SO$_4$] in the FT-1 was 1.3×10^8 cm^{-3}. In FT-2, the [H$_2$SO$_4$] was estimated to be 2.5×10^6 cm^{-3}.
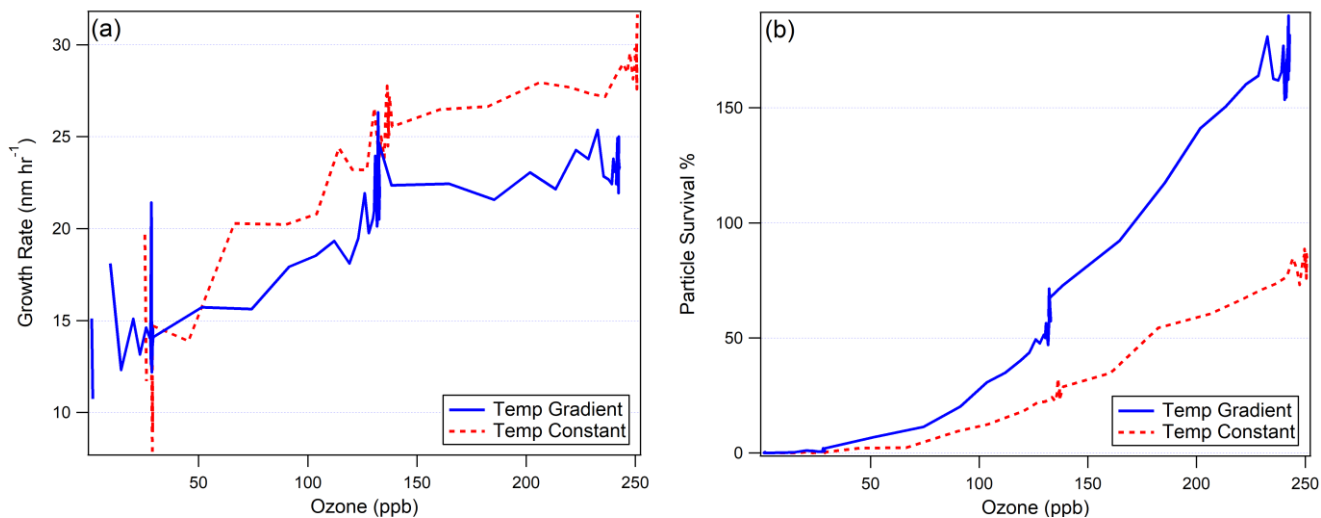
Figure 8. (a) Particle growth rate as a function of ozone concentration in FT-2 during each experiment and (b) the particle survival percentage as a function of ozone concentration in FT-2. Particle survival percentage over 100% indicates nucleation occurring in FT-2 due to an unknown heterogeneous process.